Experimental Study of Fine Particle Separation in a Multichannel Cyclone with Curvilinear Design and Theoretical Assessment under Harsh Microclimatic Conditions

Aleksandras Chlebnikovas *

Posted Date: 21 April 2026

doi: 10.20944/preprints202604.1464.v1

Keywords: multichannel; cyclone-separator; harsh microclimatic conditions; fine particles

 doi:10.20944/preprints202604.1464.v1

Article

Experimental Study of Fine Particle Separation in a Multichannel Cyclone with Curvilinear Design and Theoretical Assessment under Harsh Microclimatic Conditions

Aleksandras Chlebnikovas

Research Institute of Mechanical Science, Vilnius Gediminas Technical University, Plytinės g. 25, 10105 Vilnius, Lithuania; aleksandras.chlebnikovas@vilniustech.lt

Abstract

Contaminated gas flows are encountered in most industrial processes and require efficient removal of fine dispersed particles of various types and characteristics. Conventional cyclones are widely used under harsh operating conditions; however, their separation efficiency for fine particulate fractions remains relatively low. In this study, next-generation cyclones with a multichannel design featuring cylindrical and spiral casings are investigated, enabling particle collection efficiencies of up to 95% for particles with a diameter of 2 μm. Under harsh microclimatic conditions - particularly at high humidity levels of 70% and above, as well as elevated temperatures ranging from 50 to 200 °C - such technology is prone to clogging, necessitating complex regeneration procedures. Recent research has focused on improved channel geometries incorporating secondary peripheral flows, adapted for gas cleaning in harsh environments. Experimental results demonstrate effective removal of fine dispersed particles of glass and clay with sizes up to 20 μm at initial concentrations of 0.5-15 g/m³. The theoretical assessment of the influence of harsh gas flow conditions includes an analysis of critical flow characteristics and the mechanical forces acting on fine particles under varying temperature and humidity. The results indicate a maximum purification efficiency of up to 87.3% at an aerodynamic pressure drop of 440 Pa. The impact of harsh microclimatic conditions is most pronounced in the magnitudes of centrifugal and drag forces: with every 50 °C increase in temperature, these forces decrease on average by factors of 16 and 4.5, respectively.

Keywords: multichannel; cyclone-separator; harsh microclimatic conditions; fine particles

1. Introduction

Cyclone separators are widely used to remove particles (dust) from gas flow due to their simple design, low operating costs, and ability to operate under extreme conditions. Their principle is based on the creation of a vortex gas flow: centrifugal forces carry the particles toward the chamber walls, from where they are collected in a hopper. Such devices are suitable for operation at elevated temperatures and pressures, as well as in harsh environments (acids, abrasive gases). Numerous studies show that, despite its apparent simplicity, the flow inside a cyclone forms a complex, unsteady vortex flow that is sensitive to geometry and operating conditions. This necessitates the integration of experimental data, theoretical models, and numerical simulations when evaluating and optimizing cyclone performance [1–6].

For modern gas flow purification technologies, particle capture efficiency - including that of fine particles - is particularly important. Cyclones effectively separate large particles (typically bigger than 5–10 μm), but their efficiency decreases as particle size decreases. As noted in the literature, cyclones are capable of capturing particles with a diameter greater than 10 μm almost completely, whereas droplets or particles smaller than this size are difficult to remove using standard methods.

 doi:10.20944/preprints202604.1464.v1

Special measures are being developed to improve the capture of fine particles. For example, the introduction of a spray agglomeration system upstream of the cyclone filter increases the effective particle size due to agglomeration droplets (could be used for dry and wet post-treatment approaches). Researchers also describe designs with multi-stage separation or built-in filters, which improve the removal of ultrafine particles. However, the device geometry and flow conditions remain the primary determining factors: for particles of approximately 5 μm or smaller, it is often advisable to combine cyclones with other methods (electrostatic precipitation, chemical coagulants, etc.) [7–13].

It has been experimentally confirmed that increased particle moisture (i.e., the presence of water droplets or an adhesive layer) alters the separation characteristics. Thus, a study of an axial cyclone revealed that as material moisture increases, fine particles tend to agglomerate, increasing the fraction of large particles, and this enhances both the overall and classification efficiency for large fractions. In particular, capture efficiency increases with rising humidity for larger particles (>10 μm), whereas for smaller particles the trend may be the opposite. Thus, the humidity of the operating environment can play a dual role: it accelerates the deposition of droplets and condensed particles, but at the same time can cause additional pressure losses and unpredictability. Specific experimental results show that, all other conditions being equal, sequential humidification of the material leads to a significant increase in the proportion of large particles (due to aggregation). This feature is used in some systems that inject water or monomers upstream of the cyclone (wet cyclone separation) [14–17].

The traditional design of the cyclone separator has been extensively and thoroughly studied both experimentally and through theoretical analysis; therefore, most research focuses on investigating the qualitative properties of the technology with a view to geometrically optimizing the design. The geometry of the cyclone is a key factor determining separation characteristics and aerodynamic losses. Numerous studies have been devoted to optimizing the dimensions and shapes of cyclone components (the inlet nozzle section, the cylindrical section, the inner tube - the “vortex retainer" - and the cone). Thus, in a hybrid Computational Fluid Dynamics (CFD) - Discrete Element Method (DEM) - Artificial Neural Network (ANN) study, researchers analyzed the parameters of the inlet aspect (the ratio of the height to the width of the inlet slot), the diameter of the vortex retainer, and the height of the cylinder. It has been found that increasing the diameter or length of the vortex generator intensifies the “double-vortex” flow (Rankine-type vortex) and creates additional secondary flows, which ultimately reduces separation efficiency. The study also identified the optimal inlet aspect ratio, at which a balance between pressure and particle removal is achieved. The authors conclude that optimization requires consideration of the interaction between parameters: for example, increasing the inlet cross-sectional area without adjusting other dimensions reduces efficiency due to a decrease in vorticity [18,19].

Many studies applied multi-criteria optimization (ANOVA, MOGA), semi-empirical model and machine learning prediction to obtain a set of compromise solutions that increase efficiency without a significant change in pressure drop, energy consumption etc. Such a statistical methodology, analogous to industrial optimization, allows for the identification of effective geometries without exhaustive search [20–25].

Optimization studies are also conducted in multistage cyclone systems and designs with additional obstacles. For example, Ayli and Kocak (2024) modeled a two-stage nested cyclone with inner and outer housings, equipped with a baffle. Changing the position of this baffle radically alters the velocity distribution and pressure field: when it is moved closer to the inlet of the inner cyclone, the low-velocity zone (which aids in particle capture) expands, and the symmetry of the pressure drop is enhanced. However, the height of the partition has less of an effect—it only slightly increases the pressure difference as the height increases, and the efficiency first rises and then falls (but only by about 10%) [1]. Such studies provide practical recommendations: for internal multistage systems, it is advantageous to position the partition closer to the inlet in order to expand the low-pressure zone and improve separation [26,27].

Some innovations are also being investigated in specialized designs. For example, insertion pipes beneath the vortex generator were analyzed. It turned out that divergent and convergent inserts

 doi:10.20944/preprints202604.1464.v1

affect the flow differently: a longer insert and a larger angle of inclination expand the central low-pressure zone, while a divergent tube typically increases pressure losses. In particular, the convergent insert demonstrated better performance for very fine particles (≤5 μm), while the divergent insert performed better for larger particles (>5 μm), allowing for a reduction in pressure drop without compromising efficiency [28–30].

In most cases, technological processes on modern production lines take place under non-standard operating conditions, which are the most favorable from a technical, energy, and/or environmental standpoint. Cyclone separators are not only used under standard temperature and pressure conditions; they are widely employed in harsh, aggressive or extreme environments. As noted in reviews, their design can be adapted for high temperatures (hundreds of °C and above) and high pressures through the selection of heat-resistant materials and structural calculations. Examples include cyclone heat exchangers in the cement industry or gasification plants. CFD capabilities have been tested in such applications: for example, in the work by Nakhai et al. (2020), studies of cyclones at different temperatures were systematically reviewed. They emphasized that at high temperatures, the properties of the gas (viscosity, density) change, which affects the pressure drop and efficiency. In particular, high temperatures lead to a decrease in gas density, which can reduce particle inertia and make it more difficult to retain very fine particles [2].

A corrosive environment (acidic or abrasive gases) typically leads to corrosion and wear. Research example - cleaning of oxygen-regeneration flue gases in metallurgy: Zhang et al. (2016) demonstrated that a special high-precision cyclone can simultaneously capture hydrochloric acid (HCl) vapors and iron oxides. At gas velocities of 5-10 m/s, the separation efficiency for HCl and Fe_2O_3 exceeded 80–90%. This demonstrates that a properly designed cyclone - taking into account the aggressiveness of the mixture (use of acid-resistant materials and an air-cooled design) - can handle such tasks. At the same time, the dynamics of the parameters are similar: efficiency first increases with pressure drop, then decreases (saturation effect) [31].

Another factor is the corrosion and erosion wear of the cyclone walls. Studies show that separators are particularly susceptible to abrasive wear in the areas of the inlet nozzle and the cone. Researchers compared a standard cyclone or liquid jet separator from different materials with a modified device featuring curvilinear elements, demonstrating that the rate of wall wear increases with particle size. When the average particle diameter exceeds 40 μm, erosion increases significantly, and with very large particles, it reaches the lower part of the housing. Therefore, when designing for corrosive environments, it is important to consider the need for more durable coatings or configurations that reduce particle collisions with the walls (for example, special vortex separators that reduce peak loads) [32–35].

High gas-phase humidity is also an atypical operating condition for dry cyclones. As previously noted, high relative humidity leads to the formation of water condensate and droplets, which alters the aerodynamics. One of the latest developments is the use of spray agglomeration: a liquid is sprayed at the chamber inlet, which “coalesces” fine particles into droplets, after which the now-coalesced particles are more easily collected by the cyclone. Such technologies make it possible to improve the capture of particulate matter (PM) with a diameter of up to 10 μm (PM_{10}) and up to 2.5 μm ($PM_{2.5}$) in the moist smoke emitted by industrial facilities [36,37].

Theoretical cyclone models are based on the Navier–Stokes equations under various approximations. These models are easy to use but do not account for complex flow characteristics. Therefore, as computational capabilities have grown, numerical methods have been developed. Three-dimensional gas flow modeling that accounts for solid phase particles allows for detailed tracking of vortices and trajectories. At the same time, non-conventional operating conditions necessitate consideration of additional factors, including aggressive environments (chemically active solutions and mixtures, abrasive particles), as well as elevated temperatures and humidity. Modern modeling approaches, such as CFD, CFD–DEM, and machine learning techniques, successfully capture these effects and are widely applied in the design of advanced separators [38,39].

 doi:10.20944/preprints202604.1464.v1

Thus, contemporary research on cyclone separators encompasses a broad spectrum of methods and conditions, ranging from classical experimental studies to numerical simulations of complex unsteady flows and multi-objective optimization. The obtained results enable the development of designs with enhanced separation performance, including fine particles and humid environments, while maintaining acceptable energy consumption, ensuring the continued relevance of cyclone technology in emerging industrial applications.

Particle Separation Under Harsh Microclimatic Operating Conditions

Traditional cyclones have long been used for dust flows of various origins under normal dry-cleaning conditions, but they are not particularly effective at cleaning gases, especially those contaminated with low-dispersion pollutants (up to 20 μm in diameter) particles. The latter operate on the widely used principle of separating particles using cyclones-separator, with a cleaning efficiency of 75–85% and gas flow cleaned of particle larger than 20 microns in diameter. This is not sufficient to achieve the objectives of the Revised European Union (EU) Ambient Air Quality Directive (2024) (Directive 2024/2881) and compliance with the concentrations of bigger (PM_{10}) and smaller ($PM_{2.5}$) particles pollutant fractions stronger than earlier regulated by European countries legislation and worldwide [40–42].

Multi-channel cyclones are widely used in non-harsh operating conditions to capture fine particles ranging in size from 1 μm. Their action is based on the fact that the contaminated dust flow, passing through the cyclone channel system, is cleaned of contaminating particles not only under the action of centrifugal forces, but also by additionally trapping part of the particle formed by a "gas flow curtain" and directing the contaminants into the segmented slots of the separation chamber [43–47]. Traditional and multi-channel cyclones are more suitable for cleaning gas flows from sticky particles, but under certain conditions – high humidity, elevated temperatures, and chemical compounds in the gas flow – they become clogged, and the cleaning process stops. Their regeneration is practically impossible. Therefore, operation in such conditions requires additional scientific evaluation of the cleaning equipment with the introduction of design improvements. In the most widely used traditional and multi-channel cyclones, the uniformity of gas cleaning from particles is determined by the interaction of particles with flow-limiting surfaces. The layers of particles sediment that form on surfaces also have an impact, changing the flow and negatively affecting the particle deposition mechanism, which reduces the efficiency of particles capture [48,49].

During the movement of moist gas flow in cyclone channels, particles sediment layers are formed. This phenomenon is analyzed as the elastic rebound of contaminant particles and their adhesion to the surface, the magnitudes of the forces of these two factors, and a comparison of these forces with each other. The ratio of these forces is directly proportional to the diameter of the particles to the third power. Thus, for small particles interacting with the surface, the forces of adhesion and cohesion are significant. Studies have shown that even in a rectangular channel, intensive particles sedimentation occurs on the surface. Small particles are considered to be those that are carried along with the flows due to turbulent pulsations.

At the first stage of particles sediment formation, monolayers consisting of small particles are formed, which level the surface on which a laminar gas flow is formed, characterized by a small dispersing effect on the sediments. As sediment accumulates, larger particles can penetrate this layer and destroy these formations. When contaminated gas flow enters the cyclone separation chamber, agglomerates of small particles in the outlets of the structure hit the walls and stick to them. In this case, depending on the mass of these agglomerates and their location in the cyclone cross-section, adhesion will be uneven, and irregularities will form on the surface.

Despite the theory, large cyclones are capable of depositing even small particles, since additional inertial forces act near the surface, which arise during turbulent particle transport at large gradients of particle pulsation velocities directed towards the surface. In large cyclones, due to lower centrifugal accelerations near the surface of the confining flows, the adhesion of agglomerates consisting of small particles is less likely [50].

 doi:10.20944/preprints202604.1464.v1

Concept and Aim of Study

This study presents an analysis of gas flow dynamics under harsh microclimatic operating conditions in next-generation cyclone separators with varying geometries. The variation of aerodynamic flow parameters in curvilinear channels was examined as a function of the positioning of internal structural elements. Fractional deposition of fine particles of different origins was established through the implementation of secondary peripheral flow modifications, and a comparative assessment was conducted against configurations employing continuous structural geometries. A theoretical evaluation was performed to quantify changes in the key mechanical forces acting on particles—centrifugal, gravitational, and adhesive—as functions of aggressive gas microclimate parameters, including elevated temperature, increased humidity, and flow turbulence. The influence of these forces on gas cleaning efficiency was analyzed, revealing particle distribution patterns and identifying optimal design solutions for enhancing separation performance under extreme operating conditions.

The aim of the study is to experimentally and theoretically evaluate changes in the operating parameters of a multi-channel cyclone with different design in the harsh microclimatic conditions based on characteristic ratios, thereby determining and comparing changes in the aerodynamic parameters of the gas flow, as well as the acting particle forces and separation efficiency.

2. Materials and Methods

Sketches of the multi-channel cyclone are presented in Fig. 1. The operating principle of this type of technology can be concisely described as follows. A two-phase (gas-particles) flow enters tangentially through the inlet and enters the separation chamber, the first channel of the cyclone, which is bounded by the peripheral wall and the first curvilinear elements (curved quarter ring). The flow, flowing out of the previous channel, collides with a semi-ring wall (edge) and divides into two flows – peripheral and transit. Part of the peripheral flow enters the previous channel, thus filtering the contaminated flow with the reverse flow, and the transit flow enters the next channel in the direction of the device axis and exits the cyclone. Thus, the gas flow is distributed through channels of varying curvature and filtered through the gaps between the semi-rings.

Under the action of centrifugal forces created by the vortex flow and under the influence of the resulting filtration effect in the flow separation zone, particles settle and accumulate in the cyclone hopper, entering it through segmented ring slots.

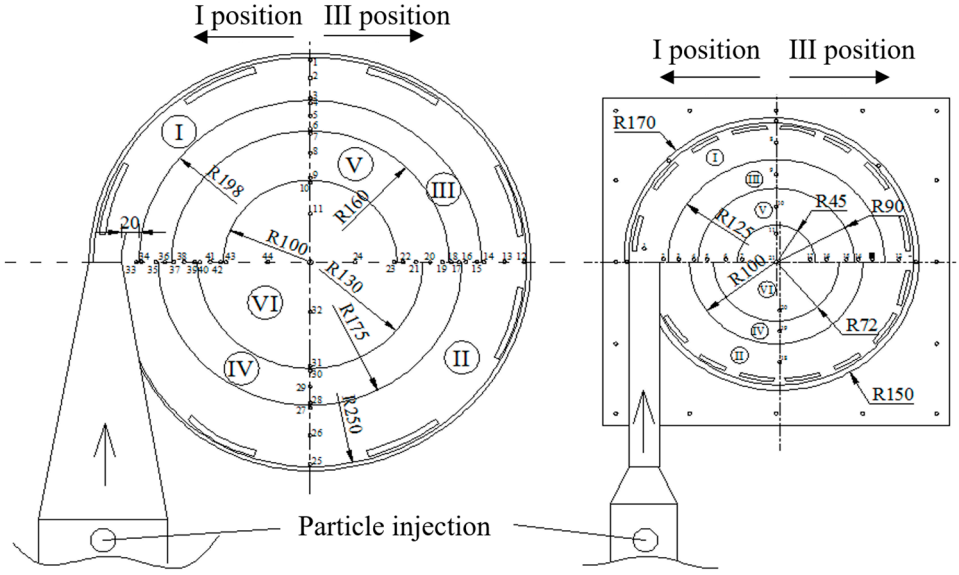

 doi:10.20944/preprints202604.1464.v1

Figure 1. Internal structures of cyclones (at semi-ring position II): I-VI –channels of the cyclone; R1-R5 – curvilinear semi-rings; 1-44 - cylindrical shell (from the left) and 1-21 (spiral shell (from the right)) - measurement points of dynamic gas flow pressure.

For both the comparative experimental and theoretical investigations, an even more advanced version of the multichannel geometry was employed, as shown in Figure 2. The operating principle remains similar; however, in this prototype, the number of interconnections between channels has been multiplied through the incorporation of openings in the internal curvilinear quarter-rings formed elements instead of semi-rings. This design promotes greater recirculation of residual particle flow from the internal channels to the external ones. Additionally, this configuration is significant for hydrothermal dilution and for extending filtration time under harsh microclimatic operating conditions.

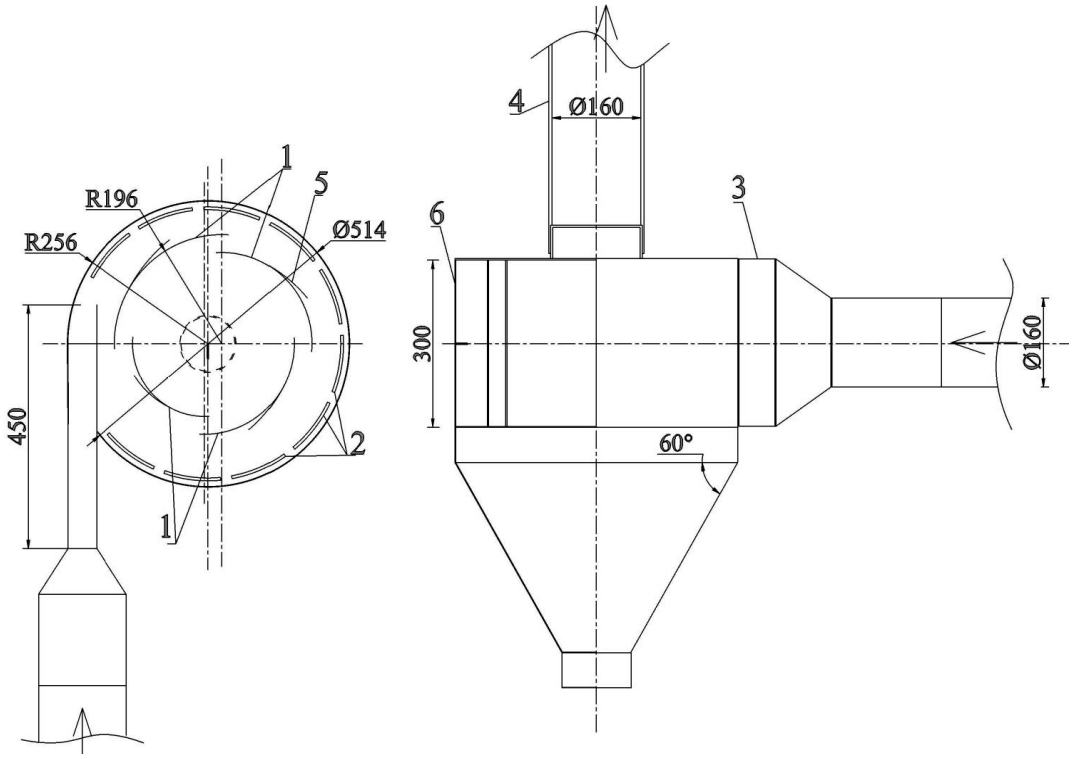

Figure 2. Optimized multi-channel's device topview (a) ir sideview (b): 1 – curvilinear quarter–rings with folded opening slots, 2 – segment circular spacings, 3 – inlet opening, 4 – cleaned gas flow outlet, 5 – folded opening slots of quarter–rings, 6 – cyclone separation chamber.

Mechanical Impact of an Harsh Microclimatic Conditions on Particles in a Cyclone Separator Channel

Purified gas flow that has passed through all the cyclone channels exits the system through the gas flow outlet. Dusty gas flow is filtered in the active zone of the channels and as a result of particles interaction during coagulation. The effect of humidity on gas flow parameters. Humidity is the amount of water vapor in the gas phase.

The partial pressure of such water vapor in the gas flow does not exceed the saturated vapor pressure under certain gas flow conditions. Water vapor formed in the gas flow reduces its density, since the molar mass of water is lower (18 g/mol) compared to dry gas flow (29 g/mol). A wet gas/vapor flow can be considered as an ideal mixture of gases, the density of each component of which corresponds to the required density of the mixture. Thus, the density value can be determined with an error of less than 0.2% when the temperature changes from -10 to 50 °C. The theoretical assessment considered cases where the temperature varied from 0 to 200 °C and the humidity from

 doi:10.20944/preprints202604.1464.v1

0 to 70%, respectively. It is assumed that the temperature of the gas flow is inversely proportional to its humidity.

The relationship between the density of the wet gas flow and the parameters of the harsh environment is described by the following Equation 1:

$$\rho_{wg} = \frac{p_{dg}}{R_{dg} \cdot T} + \frac{p_{wv}}{R_{wv} \cdot T};, \quad (1)$$

here: ϱ_{wg} – density of the wet gas flow, kg/m³; p_{dg} – partial pressure of the dry gas flow, Pa; R_{dg} – gas constant for the dry gas, equal to 287.058 J/(kg·K); T – temperature, K; p_{wv} – water vapor pressure, Pa; R_{wv} – gas constant for water vapor, equal to 461.495 J/(kg·K).

Water vapor pressure can also be calculated based on relative humidity, Equation 2:

$$p_{wv} = \varphi \cdot p_{sat.wv}, \quad (2)$$

here: p_{wv} – water vapor pressure; ϕ – humidity ratio; $p_{sat.wv}$ – partial pressure of saturated water vapor, which can be calculated using the following Equation 3:

$$p_{sat.wv} = 6.1078 \cdot e^{\frac{17.08085 \cdot t}{234.175 + t}}, \quad (3)$$

here: t –water vapor temperature, °C.

When the environment changes, the forces acting on particles in a moving gas flow also change. When gas and particles move through the cyclone channels, a drag force (resistance force) acts on the particles, causing them to move in a horizontal flow. The drag force on a particle in a gas flow can be calculated using Equation 4:

$$F_d = cS\rho \frac{\overline{u}^2}{2}, \quad (4)$$

here: c – particle drag coefficient; ϱ – gas flow density, kg/m³; S – cross-sectional area of the moving particle, m²; $\bar{u}$ – mean gas flow velocity, m/s.

The change in drag force due to operating parameters under harsh environmental conditions was estimated in similar cases by calculating the gas flow density.

The force generated by the gas flow acting on a particle is proportional to the square of the gas flow velocity, i.e., F~v², so when the gas flow velocity in the cyclone decreases, the force decreases by a factor of two. For this reason, the separation of particles from the surface decreases significantly with distance from the cyclone inlet and practically disappears at a distance of 10–15 mm.

The centrifugal force acting on a particle characterizes the magnitude of the force under which a characteristic particle is subjected to when it moves in the cyclone channel around the axis of the device. The magnitude of this force is determined by the inertia of the moving particle, since the direction of its movement in a multi-channel cyclone is constantly changing. The magnitude of this force is calculated using Equation 5:

$$F_c = \frac{\frac{4}{3}\pi \rho_d r_p^3 v^2}{r_{cs}}, \quad (5)$$

here: ϱ_p – particle density, kg/m³; r_p – particle radius, m; v – gas flow velocity, m/s; r_{cs} – radius of the cyclone channel, m.

The gas flow moving in a multi-channel cyclone is turbulent, so the drag force Equation 6 is as follows:

$$F_d = 0.173 d_p^2 (u - v)^2 \rho, \quad (6)$$

here: μ – dynamic viscosity coefficient; u – gas flow velocity in the cyclone, m/s; v – particle velocity in the cyclone, m/s; d_p - particle diameter, m.

Using the ratio of dynamic and kinematic viscosity coefficients $\mu = \nu\rho$, Equation 6 for the resistance force to a turbulent gas flow can be written as follows (Equation 7):

$$F_d = 0.173 d (u - v)\, Re\, \mu, \quad (7)$$

When a particle moves through the cyclone channel, it is affected not only by the centrifugal forces of the gas flow, but also by the gravitational forces of the particles themselves, which have mass. This force changes the trajectory of the particles, causing them to be separated from the gas flow and deposited in the cyclone hopper. The standard expression of the force of gravity acting on the body under consideration was used for the assessment (Equation 8):

$$F_{gr} = 4 \frac{\pi \left(\frac{d_p}{2}\right)^3}{3} \cdot \rho_d \cdot g, \quad (8)$$

 doi:10.20944/preprints202604.1464.v1

It is assumed that the density of the particles is 1000 kg/m^3 and that the particles are spherical in shape. The gravitational force acting on particles measuring 1, 2.5, 5, 10, and 20 micrometers was evaluated.

Adhesion phenomena occur when bodies come into contact and are the result of their molecular interaction, which manifests itself when a particle comes into direct contact with the surface. The adhesive force depends on the contact surface area, since molecular interaction is proportional to the contact area.

The detachment of finely dispersed adhered particles from the surface under the action of a gas flow occurs in several stages. First, the larger upper particles detach, followed by the smaller ones, i.e., the adhesive forces of the layer are overcome. The detachment of the upper particles is possible when $F_{adh}>F_{cohesion}$. The detachment of particles under the action of self-adhesion forces is called erosion. When $F_{adh}<F_{cohesion}$, the layer detaches along the surface – the boundary of the layer. In this case, the adhesive forces are overcome, and this process is called denudation.

Despite electrical and capillary forces, the true shape of particles, and other factors, the magnitude of the adhesive force is expressed by the dependence:

$$F_{adh} = \frac{h\omega}{16\pi z_0^2} d_p = \frac{h\omega}{8\pi z_0^2} r_d, \quad (9)$$

here: hω – Lifshitz–van der Waals constant, J; z_0 – distance between the particle and the plane surface at which adhesion forces are maximal; r_p – particle radius, m.

Studies have shown that at a distance of 4×10^{-10} m, the adhesive force is at its maximum and equals:

$$F_{adh} = 2.4 \cdot 10^{-7} r_d, \quad (10)$$

The adhesive force decreases proportionally to the square of the surface area. Therefore, small particles have a larger surface area compared to large particles, and their adhesive force is greater than that of large particles. For this reason, less force is required to detach large particles from the surface than to detach small dispersed particles. Therefore, large particles detach from the surface more easily and at lower gas flow rates.

Adhesion forces were estimated for particles with sizes of 1, 2.5, 5, 10, and 20 μm, assuming that the adhesion force is maximum in all cases.

Aerodynamic studies of dynamic pressure resistance were conducted using a single-phase gas flow. The cyclone gas cleaning efficiency was evaluated by introducing dried glass and clay particles up to 20 μm in size. Dynamic gas flow pressures were measured using a Pitot–Prandtl tube connected to a multifunctional Testo-400 meter (Testo, Titisee-Neustadt, Germany) (temperature measurement range: 20–70 ◦C, accuracy ±0.2 ◦C, velocity measurement range: 1–30 m/s, accuracy ±0.05 m/s, dynamic pressure measurement range: 1-2000 Pa, accuracy ±0.5 Pa). Openings in the covers of the cyclone separation chambers allowed the insertion of the dynamic pressure measurement tube at critical locations: in the semicircular and peripheral boundary layers, 2 mm from the surface of each curvilinear semicircle, in the first channel, and in the inter-ring gap (at the midpoint of the distance). The measured axial dynamic pressure corresponded to the sixth channel. The aerodynamic resistance of the six-channel cyclone (pressure difference between the inlet and outlet static pressures) indicates the pressure loss experienced by the gas flow through the multichannel cyclones. Aerodynamic resistance was investigated using multifunctional meters equipped with differential pressure sensors ("Testo 440 dP"). Technical data of the Testo 440 dP multimeter: measuring ranges of 0–50 m/s, −20–+70 °C, 5–95% RH, and 700–1100 hPa; accuracy ± (0.03 m/s + 4% of the measured value (m.v.)) (0 to 20 m/s), ±0.5 °C (0 to +70 °C), ±3.0% RH (10 to 35% RH) and ±2.0% RH (35 to 65% RH), and ±3 hPa; resolution 0.01 m/s, 0.1 °C, 0.1% RH, and 0.1 hPa.

Dynamic and static pressure tests were repeated at least five times over periods of no less than 30 seconds, during which the measured values varied by no more than ±3%, in order to avoid systematic errors and reduce the uncertainty in the averaged test results.

For the cylindrical cyclone, the maximum flow rate was selected corresponding to an inlet velocity of 21.9 m/s. In the spiral cyclone, an axial fan was installed, for which gas flow regulation is not provided; therefore, a nominal performance was chosen, corresponding to an inlet velocity of

 doi:10.20944/preprints202604.1464.v1

17.8 m/s. Three positions of the curvilinear semicircular elements were investigated (Figure 1, denoted as Positions I, II, and III), and dynamic pressure and aerodynamic resistance measurements were performed accordingly. This adjustment procedure aimed to determine the optimal semicircle arrangement to achieve the best aerodynamic characteristics of the device and gas flow purification efficiency. During the adjustment, the semicircular elements were displaced 10 mm to the left for Position I and 10 mm to the right for Position III relative to the reference Position II (Fig. 1). The adjustments involved repositioning the second semicircle to 175 mm radius in the cylindrical cyclone and 100 mm in the spiral cyclone; the third semicircle to 160 mm and 90 mm, respectively; and the fourth semicircle to 130 mm and 72 mm.

For experimental determination of the six-channel cyclone's efficiency in cleaning contaminated gas flows, the particles typical of the construction and materials processing industries were selected. To feed particles into the inlet gas flow for the efficiency tests, a Palas RBG 1000 solid particle disperser (Palas, Germany) was used to generate and inject a polluted gas flow from powders as a simulated emission source. The concentrations of particles were quantified using the Welas digital 3000 H instrument both upstream and downstream the cyclone-separator installation. The removal efficiency of the technology was studied based on the concentration of particulate matter. The mass concentration was only used to determine the dosage, i.e., the number of particles delivered to the inlet gas duct. Laser sensors were used in the pre- and post-cleaning sections to capture samples and quantify the particle size composition. A detailed grain composition of the tested particulate matter is presented in Table 1.

Table 1. Particles dispersion content.

Parameter	Glass	Clay
Particle diameter at 10% cumulative volume, μm	2.66	1.95
Particle diameter at 50% cumulative volume, μm	9.26	7.52
Particle diameter at 90% cumulative volume, μm	18.58	16.25
Median diameter, μm	10.02	8.95

The bulk density of the glass sample was 1650 kg/m^3, and the particle density was 2430 kg/m^3. The bulk density of the clay sample was 1350 kg/m^3, and the particle density was 2560 kg/m^3.

The openings (window-shaped zones) in the curvilinear elements allow the gas flow to re-enter the preceding channel section. Each window is cut below the horizontal symmetry line of the semicircle to ensure that particles specifically enter the adjacent wall-limiting channel, while not obstructing the passage of clean gas flow further toward the outlet. The window design also allows for adjustment by varying the curvature width of the cutout. In the experiments, all four quarter-rings were equipped with windows, with a curvature width of 20 mm. Since the experiments were conducted with glass and clay dusts of different origins, after tests with the first type of sample, the entire system—including hoses and the cyclone structure - was cleaned (regenerated) by blowing through it with a high-velocity gas flow.

3. Results

The dynamic and kinematic viscosities of the gas play a significant role in the flow of harsh gas flows. Since kinematic viscosity is directly proportional to dynamic viscosity, correlations that account for temperature and density parameters are applied. According to established principles of molecular physics and thermodynamics, the dynamic viscosity of an harsh microclimatic conditions vary primarily with the gas temperature, whereas the kinematic viscosity depends on both the gas temperature and density (Menter, 1994).

 doi:10.20944/preprints202604.1464.v1

For the study of gas dynamic viscosity under harsh microclimatic conditions, baseline values were first calculated under standard conditions, i.e., at 0 °C and 0 % relative humidity, with a pressure of 101.3 kPa. Under these conditions, the dynamic viscosity is 17.17 μPa·s, and the kinematic viscosity is 13.28 mm²/s. Additional cases were calculated using thermodynamic–microclimate correlations, with the results presented in Table 2.

Table 2. The gas flow parameters depending on the characteristics under harsh microclimatic conditions.

Parameter	μ_g	ν_{wg}	Dew point
Dimensions	μPa * s	mm²/s	°C
At normal conditions (0 °C and 0% RH)	17.17	13.28	-
t = 50 °C, ϕ = 95% RH	19.26	16.44	49.0
t = 100 °C, ϕ = 95% H	21.25	14.11	98.6
t = 150 °C, ϕ = 80% RH	23.16	8.25	142.0
t = 200 °C, ϕ = 70% RH	24.99	4.26	184.0

The temperature and relative humidity of gas flow under harsh microclimatic conditions frequently vary during the operation of a multichannel cyclone. To investigate this, a theoretical study was conducted for relative humidities of 0%, 50%, and 95%, while the temperature varied between 20 °C and 200 °C.

As previously noted, the dynamic viscosity depends solely on the gas temperature, so this parameter was evaluated only at different temperatures. Under standard conditions (20 °C gas flow temperature) and relative humidity ranging from 0% to 95%, the dynamic viscosity is 18.02 μPa·s.

Theoretical analysis of gas flow under harsh microclimatic conditions showed that at 50 °C and 95% relative humidity, the density of the wet gas flow is 1.172 kg/m³. Under these conditions, the dynamic viscosity of the gas flow is 19.26 μPa·s, the kinematic viscosity is 16.44 mm²/s, and the dew point temperature is 49 °C.

Such harsh operating conditions are typical in thermal boiler plants, where flue gases from a biomass boiler pass through coolers (economizers). In this case, the gas temperature ranges from 50 °C to 100 °C, and the dynamic viscosity of the gas flow under harsh microclimatic conditions is higher than under standard conditions by 7% and 18%, respectively. At 100 °C, the maximum possible relative humidity remains 95 %, with a dynamic viscosity of 21.25 μPa·s and a kinematic viscosity of 13.94 mm²/s. The dew point temperature is close to the gas flow temperature (98.6 °C), indicating that the gas flow is supersaturated and condensation occurs even on slightly cooled surfaces.

In the theoretical study, at the highest temperatures considered (150 °C and 200 °C), the dynamic viscosity reached 23.16 μPa·s and 24.99 μPa·s, respectively, and the kinematic viscosity ranged from 16.53 mm²/s to 19.52 mm²/s. Dew point temperatures in these cases were 100.8 °C and 101.7 °C. For temperatures of 150 °C and 200 °C, the dew point exceeds 100 °C, which is thermodynamically impossible, indicating a supersaturated environment; therefore, further variations were not evaluated. Such gas temperatures are encountered in industrial flue gas flows after combustion processes (boilers, autoclaves), where the relative humidity may reach up to 10 % after the boiler, or 5–30% after various drying furnaces when wet raw materials or injected reagents/special solutions are used.

Kinematic viscosity of the gas flow under harsh microclimatic conditions is inversely proportional to relative humidity in the 50–100 °C temperature range. Exceptions include cases with 0% relative humidity, where kinematic viscosity is directly proportional to the gas temperature.

 doi:10.20944/preprints202604.1464.v1

Another notable exception is the 50–100 °C gas flow at 50% relative humidity: kinematic viscosity initially increases with temperature up to 100 °C, then decreases. This behavior is associated with water evaporation, where water transitions to the gas phase, reducing friction forces between particles. At 95% relative humidity, the critical temperature is 61 °C, above which kinematic viscosity decreases with increasing temperature. This indicates that in highly humid gas flows, evaporation occurs more intensely, reducing friction at temperatures lower than the water boiling point (100 °C).

At 20 °C and 0% relative humidity, the kinematic viscosity is 14.96 mm²/s. At 50% and 95% relative humidity, the values decrease by 0.7% and 1.3%, respectively. At higher temperatures (50 °C and 100 °C), the viscosity increases significantly (by 1.1–1.2 times), yielding 17.62 mm²/s, 16.98 mm²/s, and 16.44 mm²/s at 0%, 50%, and 95% humidity. For the exceptional temperature ranges, dry gas kinematic viscosity reaches 22.45 mm²/s, and for 50% and 95% humidity, 16.99 mm²/s and 13.94 mm²/s, respectively. At 150 °C and 200 °C, kinematic viscosity at 0% humidity increases on average by 1.22 times per 50 °C interval, reaching 33.49 mm²/s at 200 °C. At 200 °C and 6.6% relative humidity, kinematic viscosity increases by 40% compared with the 100 °C case at 95% humidity.

The behavior of gas flow under harsh microclimatic conditions in the improved multichannel cyclone involves complex aerodynamic and mechanical processes. Peripheral and transitional flow interactions occur, generating centrifugal, gravitational, and adhesive forces on the particles, as well as drag, capillary, and electrostatic forces. Evaluating these processes and their impact on the operation of the improved multichannel cyclone is essential for the theoretical study of particle removal from gas flow under harsh microclimatic conditions.

Theoretical studies analyzed different effect of harsh microclimatic conditions on particle-laden gas parameters in the improved multi-channel cyclone, whose schematic is shown in Figure 3. The particles contacted with the hot-humid gas flow are distributed within the cyclone channels. The forces acting on the particles are most effectively analyzed in the initial inlet zone of the first channel, where they are assumed to reach maximum values. Adhesion effects should be evaluated on vertical surfaces, as the separation chamber channels are composed of curvilinear elements (curved vertical plates) continuously exposed to the gas flow. Adhesion forces can then be compared with gravitational and centrifugal forces. This results in several possible outcomes: particles may remain adhered to the wall, be carried out with the cleaned gas through the outlet, or fall to the bottom of the separation chamber or into the cyclone collection bin under the action of gravity.

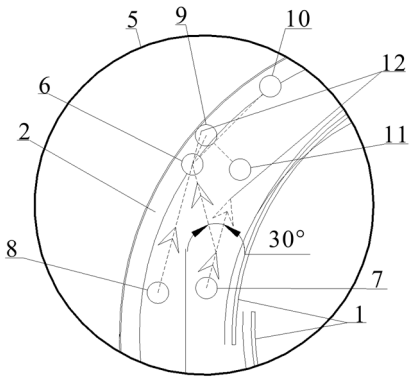

Figure 3. Newly designed multi-channel cyclone: a) top view; b) the forces acting on the particles moving through peripheral and transitional flows profile; 1 – configured curvilinear elements (curved quarter-ring-formed) elements; 2 – outer ringed continuous slit; 3 – dusted gas flow inlet duct; 4 – cleaned gas flow removal outlet duct; 5 – part of the theoretical research; 6 – particle interacting with peripheral and transitional flows; 7, 8 – incoming (transitional) and reciprocal (peripheral) particle; 9 – particle is exposed to adhesion force; 10 – particle falling through a outer ringed continuous slit, acting on the gravity force; 11 – slight bounce of particles from the surface; 12 – particle trajectory in the absence of transitional and peripheral interactions.

As particles move through the cyclone channels, they are entrained by the gas flow, which generates a drag force causing particle motion in the horizontal flow direction. The magnitude of the

 doi:10.20944/preprints202604.1464.v1

force exerted by the gas flow on a particle is proportional to the square of the gas velocity, i.e., $F \sim \bar{u}^2$; therefore, as the gas velocity decreases within the cyclone, the force decreases quadratically. Consequently, particle detachment from surfaces significantly diminishes along the cyclone channel and practically vanishes at distances of 10–15 mm from the inlet. According to the laws of curvilinear mechanics, the drag force is directly proportional to the particle drag coefficient, its cross-sectional area, the gas density, and the square of the mean gas velocity.

Applying this relationship to fine particles in the improved multi-channel cyclone under non-harsh microclimatic conditions, the drag force was found to be 12.07 nN. For particles moving in a gas flow under harsh microclimatic conditions with temperatures ranging from 0 °C to 200 °C and relative humidity from 0% to 95%, the force acting on the particle decreases only by 1–1.5%. Therefore, the effect of harsh microclimatic conditions on this force can be considered negligible.

The centrifugal force acting on a particle describes the force experienced by a characteristic particle moving around the cyclone axis. Its magnitude is determined by the inertia of the moving particle, as the particle trajectory continuously changes in the multichannel cyclone. In general, the centrifugal force is directly proportional to the particle density, the cube of its radius, and the gas velocity, and inversely proportional to the radius of the cyclone channel through which the particle moves.

To evaluate the centrifugal force of gas flow in harsh microclimatic conditions, it was assumed that particle density equals 1000 kg/m³, and particles of 2.5 μm and 10 μm diameters were analyzed. Particles of 1 μm diameter experience a negligibly small centrifugal force and are therefore not considered. According to the theoretical results, for a gas temperature of 20 °C and 50% relative humidity, 2.5 μm and 10 μm particles experience centrifugal forces of 5.2 pN and 335.1 pN, respectively, with a force ratio of 64.4. Calculations at a constant gas density were also performed for 95% relative humidity and 100 °C. The results reflect the recalculated gas velocities, which vary due to temperature and humidity: 12 m/s under non-harsh microclimatic conditions, 10.7 m/s at 100 °C, and 11.7 m/s at 200 °C. At 100 °C, centrifugal forces decrease by approximately 20%, yielding 4.2 pN for 2.5 μm particles and 266.7 pN for 10 μm particles. At the maximum gas temperature of 200 °C, the centrifugal forces increase slightly compared to 100 °C, reaching 5.0 pN and 317.7 pN for 2.5 μm and 10 μm particles, respectively.

Peripheral–transit flow interactions in the improved multichannel cyclone influence the forces acting on particles in the gas flow under harsh microclimatic conditions, including centrifugal forces. Theoretical studies examined the centrifugal–filtration forces acting on 2.5 μm and 10 μm particles.

Consider a case where a particle (II) (Figure 3, No 8) enters the first channel of the improved cyclone along the main trajectory (transit flow), while another particle (I) (Figure 3, No 7) returns from the fourth channel along a peripheral trajectory. Both particles collide within the first channel. Assumptions for this analysis include: the centrifugal force is uniform along the first channel; the particle trajectories are parallel; particle velocities are equal; and the peripheral particle (I), acted on by centrifugal force, is deflected 30° toward the outer wall upon entering the first channel. Other forces are neglected.

According to mechanics phenomena, the centrifugal force of particle I moving in the peripheral flow is reduced as follows: $\cos\alpha \cdot F_c = 0.866 \cdot F_{c.p2}$, where α is the trajectory deflection of particle I, and $F_{c.p2}$ is the centrifugal force acting on particle II in the transit flow.

The centrifugal–filtration force acting on particle II was determined based on the previously calculated centrifugal forces. For harsh microclimate conditions, when the gas temperature is 200 °C and relative humidity is 6.6%, this force decreases by approximately 15%, reaching 4.3 pN and 275.1 pN for 2.5 μm and 10 μm particles, respectively. Assuming that the entire centrifugal–filtration force of particle I contributes to decelerating particle II, the resulting force is: F_c–cos $\alpha \cdot F_c$. This force will decrease by approximately 7 times, reaching 0.7 pN and 42.6 pN for the particles with diameters of 2.5 μm and 10 μm, respectively.

These results indicate that filtration in the improved multichannel cyclone reduces the centrifugal force from the incoming gas flow under harsh microclimatic conditions and increases the

 doi:10.20944/preprints202604.1464.v1

force on particles moving from the previous channel with the peripheral flow. It should be emphasized that specific assumptions and conditions were applied, idealizing the scenario.

In addition to centrifugal forces from the gas flow, particles moving through the cyclone channels experience their own mass and gravitational forces. Acting vertically downward, gravity directs particle trajectories toward the separation chamber bottom. Particles entering the segmented annular gaps are separated from the gas flow and deposited in the cyclone collection bin. According to the general expression for gravitational force, this force is directly proportional to the cube of the particle diameter and its density.

As the dust-laden gas flow moves through the cyclone channels, the particles within it are acted upon by the flow generated by the centrifugal fan at the specified flow rate. The calculated changes in the pressure force at an average velocity in the first channel of 12 m/s in the cyclone under various harsh microclimatic conditions are presented in Table 3.

Table 3. Drag force acting on particles under harsh microclimatic gas flow conditions.

Gas flow characteristics (temperature, humidity)	Pressure force, mN
at normal conditions (0 °C and 0% RH)	1.07
t = 50 °C, ϕ = 95%	1.02
t = 100 °C, ϕ = 95%	1.16
t = 150 °C, ϕ = 80%	1.58
t = 200 °C, ϕ = 70%	2.37

In the channels of the multi-channel cyclone, the Reynolds number of the gas flow exceeds 2300, indicating a turbulent flow regime. Consequently, using Equation 8, the changes in the calculated pressure force are evaluated under various harsh microclimatic conditions. It is assumed that the particle is spherical, and the average gas flow velocity in the first cyclone channel is 12 m/s. The calculated results are presented in Figure 4.

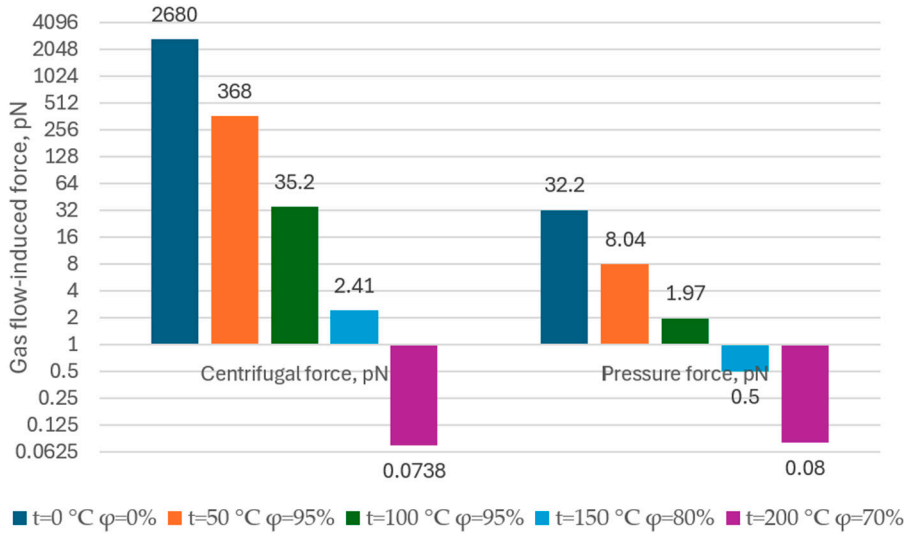

Figure 4. Logarithmic variation of particle pressure and flow-induced centrifugal forces under harsh environmental conditions.

In harsh microclimatic conditions, the particles interact with water vapor and other chemical compounds, leading to an increase in particle mass and, consequently, in gravitational force acting on them. For this purpose, the gravitational force acting on particles of different diameters (1 μm, 2.5 μm, and 10 μm) and densities (500–2000 kg/m³) in gas flow under harsh microclimatic conditions was

 doi:10.20944/preprints202604.1464.v1

determined. It is assumed that the particles are spherical, and particle saturation in the gas flow is neglected.

The analysis showed that the smallest selected particle (1 μm diameter) is subjected to a gravitational force of 0.003–0.01 pN, depending on particle density (500–2000 kg/m³). As density increases, the gravitational force increases linearly; however, the maximum relative difference was observed between the 500 kg/m³ and 1000 kg/m³ cases. For particles with diameters equal to or greater than 2.5 μm, the force increases rapidly, with the average difference between these forces being approximately 11.7-fold. Particles with a 10 μm diameter experience a gravitational force eight times greater than that on 2.5 μm particles. Specifically, the gravitational force acting on 1 μm particles is 0.01 pN, while for 10 μm particles it reaches 10.3 pN. Similar to other acting forces, a significant increase in force magnitude occurs for particles larger than 2.5 μm.

Adhesion phenomena arise from contact between bodies and result from molecular interactions that occur during direct contact between a particle and a surface. Adhesion force depends on the contact area, as molecular interactions are proportional to this area. In the improved multichannel cyclone, adhesion force is evaluated between particles moving in the gas flow and vertical internal surfaces, i.e., the peripheral walls of the separation chamber and quarter-ring elements with bent plates.

Fine particles have a larger surface area relative to their volume than coarse particles, resulting in greater adhesion forces. Therefore, detachment of coarse particles from surfaces requires a smaller force compared to the detachment of fine particles. Consequently, coarse particles are removed from surfaces more easily and at lower gas flow velocities.

The removal of fine particles adhering to vertical surfaces by the gas flow occurs sequentially: larger upper particles are detached first, followed by smaller particles, thereby overcoming the adhesion forces of the particle layer. Detachment of only the upper particles is possible when $F_{adhesion} > F_{cohesion}$. Particle detachment under the action of auto-adhesion forces is referred to as erosion. When $F_{adhesion} < F_{cohesion}$, detachment occurs along the surface layer. In this case, adhesion forces are overcome, and this process is referred to as denudation.

In this theoretical study, the adhesion force was evaluated based on its maximum magnitude, i.e., when the gap between the particle and the planar surface is equal to $4 \cdot 10^{-10}$ m.

Based on the results, it can be stated that the adhesion force acting on 1 μm and 2.5 μm particles in the gas flow under harsh microclimatic conditions is greater than the gravitational force. The maximum adhesion force on a 1 μm particle is 0.24 pN, and on a 2.5 μm particle is equal to 0.6 pN. However, as particle diameter increases, the force grows proportionally, and compared with other forces, the relative significance of adhesion decreases. Therefore, it can be concluded that such fine particles are more prone to accumulate on the vertical internal elements of the enhanced multi-channel cyclone, since in this case the adhesion force exceeds gravitational force. Conversely, particles with diameters equal to or greater than 10 μm can be easily detached from surfaces even under the influence of gravity alone, and the adhesion force is equal to 2.4 pN (Figure 5).

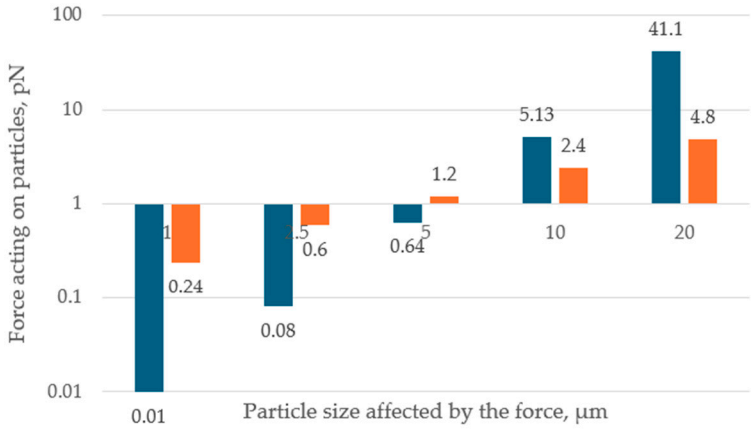

 doi:10.20944/preprints202604.1464.v1

Figure 5. Gravitational and adhesion forces on different particle sizes under harsh environmental conditions

The theoretical analysis of adhesion can be approached as a comparison of the forces responsible for particle retention versus detachment from the surface. For this study, particles of 2.5 μm and 10 μm diameter with a density of 1000 kg/m³ were selected.

A particle with a diameter of 2.5 μm moving under harsh gas flow conditions experiences a centrifugal filtration force of 0.7 pN, while the adhesion force is 14.3% lower. Therefore, the adhesion force is insufficient to retain the particle on the vertical surface of the first channel of the cyclone separation chamber; consequently, the particle rebounds and continues along the cyclone channel. A similar rebound occurs for a 10 μm particle, as the centrifugal–filtration force in this case is 19.3 times greater than the adhesion force.

It was found theoretically that a 10 μm particle can adhere to the surface and remain there only when the velocity of the harsh gas flow in the first channel does not exceed 2.8 m/s at 200 °C and a relative humidity of 6.6%, i.e., when the adhesion force (2.4 pN) exceeds the centrifugal–filtration force (2.39 pN). For smaller particles, such as a 2.5 μm particle, adhesion occurs if the flow velocity decreases from 11.7 m/s to 11.0 m/s, at which point the adhesion force (0.6 pN) exceeds the centrifugal–filtration force (0.59 pN).

The gas flow in the enhanced multi-channel cyclone is turbulent; therefore, the drag force, according to applied aerodynamic physical expressions, is directly proportional to the particle diameter squared, the gas density, and the square of the relative velocity between the particle and the gas in the first channel of the cyclone.

Applying the relationship between dynamic and kinematic viscosity $\mu=\nu\cdot\rho$, the Reynolds number of the particle is calculated for evaluating drag in turbulent gas flow under harsh microclimatic conditions. Assumptions include spherical particle shape and a particle speed 5% lower than the gas flow velocity. Drag force was calculated for particles of 1 μm, 2.5 μm, and 10 μm, with the gas velocity in the first channel at 11.7 m/s. The analysis indicates that the influence of harsh gas flow on the drag force is negligible, with variations of only 0.001 pN arising from temperature and humidity changes; therefore, this effect can be neglected relative to neutral gas conditions. For a 1 μm particle, the drag force is 0.076 pN, and the Reynolds number is 0.030. For a 2.5 μm particle, the drag increases 6.3 times to 0.47 pN, and the Reynolds number rises 2.5 times to 0.075. For a 10 μm particle, the drag increases significantly to 7.56 pN, with a Reynolds number of 0.299. It is evident that particles larger than 2.5 μm experience a substantial increase in drag force.

The drag force acting on particles in harsh gas flow conditions is 1.49-fold and 5.63-fold lower than the centrifugal–filtration force for 2.5 μm and 10 μm particles, respectively. These results indicate that drag cannot be neglected, as it affects particle trajectories in the multi-channel cyclone by slowing particles in the gas flow. While larger particles experience higher drag, the ratio of drag to centrifugal–filtration force for 2.5 μm and 10 μm particles is 16 and 60.9, respectively. Furthermore, doubling particle diameter approximately quadruples drag force, reflecting its dependence on the particle cross-sectional area exposed to the flow.

When in contact with a non-wetting flat surface, capillary adhesion is directly proportional to the surface tension of the liquid layer (here, water on the cyclone's metal walls), the distance between the particle and the surface, and the wetting angle. Auto-adhesion, occurring between particles already adhered to the surface and water droplets on their surface, is approximately half as strong as adhesion, since it acts only on the external portion of the particle's surface (Figure 6).

Theoretical investigations evaluated the maximum adhesion and auto-adhesion forces acting on a particle under harsh microclimatic conditions. It was assumed that the particle enters the primary gas inlet and moves through the first channel at various angles relative to the cross-sectional centerline. Water droplets were assumed to be evenly distributed across the peripheral wall, with a temperature of 200 °C and surface tension of 37.8 mN/m. The wetting angle was determined from the trajectory of the particle relative to the channel curvature in each case. The particle-surface distance was $4\cdot10^{-10}$ m, consistent with molecular adhesion analysis, where attractive forces dominate over repulsive forces.

 doi:10.20944/preprints202604.1464.v1

Results indicate that the capillary adhesion and auto-adhesion forces act more strongly on transient particles than on peripheral ones, due to lower wetting angles for particles entering the cyclone. Maximum auto-adhesion force was 94.5 pN, and adhesion force was 189 pN, acting on transient particles with wetting angles from 6° to 32°. Peripheral particles experienced forces on average 4.5 % lower, with adhesion peaking at 185.9 pN at 12°. The analysis shows that capillary adhesion is strongest in regions of highest curvature along the peripheral wall, increasing as particles travel further along the channel. Consequently, adhesion due to capillary forces is stronger at the end of the cyclone channels than at the beginning, assuming uniform flow and characteristics throughout the channel.

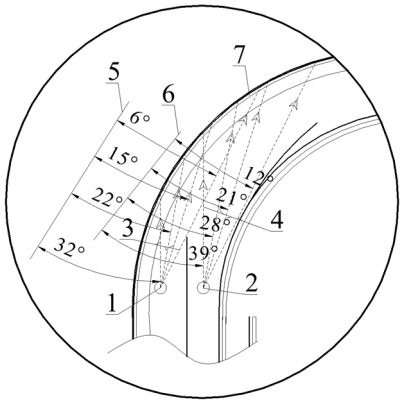

Figure 6. Peripheral and transitional moving particles◎trajectories and irrigation angles for adhesion–capillary force analysis (disregarding particle sizes) in the 1st newly designed cyclone channel: 1 – the particle moving through the transitional gas flow entering the primary gas inlet of multi-channel cyclone; 2 – the particle moving through the peripheral gas flow, returning from the 4th to the 1st channel; 3 and 4 – transitional and peripheral particle trajectories and corresponding irrigation angles; 5 and 6 – determining the curvature of the 1st channel for the irrigation angle; 7 – a layer of water droplets on the peripheral multi-channel cyclone wall.

Compared to other forces acting on a particle, the capillary adhesion force is significant in magnitude, slightly lower than the centrifugal–filtration force, and greater (by more than an order of magnitude) than the drag or gravitational forces.

Fine particles entering a multi-channel cyclone in harsh gas flow conditions come into contact with its internal surfaces. The electrical charges present on the particle surfaces attract charges of opposite sign on the cyclone walls. Based on previous studies (Fletcher, Briggs, Ferguson & Gillen, 2008; Ibrahim, Burk, Etzler & Neuman, 2000), when evaluating the electrical component of the adhesion force, it is assumed that, upon particle detachment from the cyclone surface, a residual charge remains on the wall equal in magnitude but opposite in sign to that of the particle. In this case, the electrical adhesion force is directly proportional to the particle charge squared during detachment and inversely proportional to the contact surface area (cm²) of the particle with the multi-channel cyclone wall (Figure 7).

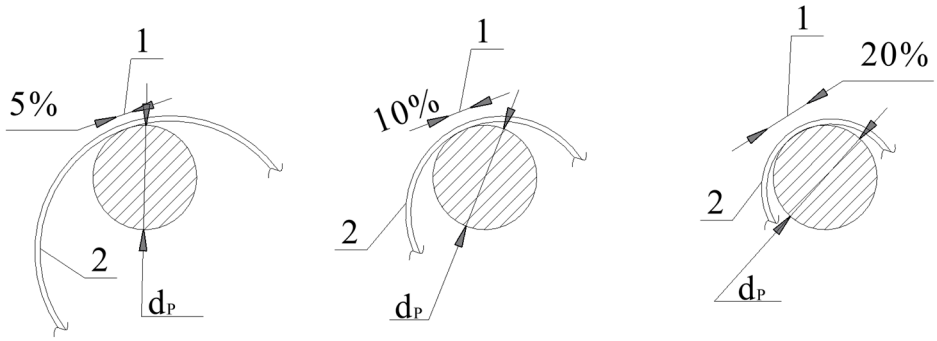

 doi:10.20944/preprints202604.1464.v1

Figure 7. Interaction of a diameter of charged particle (d_p) with surface of varying curvature expressed as 1) a percentage (5%, 10% and 20%) of the total particle surface in 2) a multi-channel cyclone body.

To standardize the measurement units of particle charge, a multiplier of 2π is applied. A simplified case is considered, neglecting the surface and subsurface properties of both contact interfaces. For the theoretical investigations, the fine particles were assumed to be ideally spherical, resulting in surface areas of $3.14 \cdot 10^{-8}$ cm², $1.96 \cdot 10^{-7}$ cm², and $3.14 \cdot 10^{-6}$ cm² for 1 μm, 2.5 μm, and 10 μm particles, respectively. Based on surface curvature, the contact area for each particle was determined. The particle charges were assumed as follows: 1 μm – $20 \cdot 10^{-15}$ Cu, 2.5 μm – $40 \cdot 10^{-15}$ Cu, and 10 μm – $100 \cdot 10^{-15}$ Cu, corresponding to the measured perpendicular charge of a glass particle detached from a metallic surface.

Under these conditions, the electrical adhesion force at 5% contact area (i.e., the smallest considered case) is $1.6 \cdot 10^{-6}$ pN, $1.02 \cdot 10^{-6}$ pN, and $4 \cdot 10^{-7}$ pN for fine particles of 1 μm, 2.5 μm, and 10 μm, respectively. As the contact area increases, the particle charge is proportionally transferred to the surface, reducing the electrical adhesion force, which ranges between 2–$8 \cdot 10^{-6}$ pN. When the contact area reaches 20% of the total particle surface, the adhesion electrical force acting on 1–10 μm fine particles becomes extremely small, not exceeding $4 \cdot 10^{-7}$ pN. Based on these results, it can be concluded that, for sufficiently small particle charges, the electrical adhesion force is negligible and does not significantly influence particle adhesion in the multi-channel cyclone, since other forces are three to four orders of magnitude greater.

Additional studies considered the peak particle charge, at which the electrical force exceeds the adhesion or centrifugal–filtration forces. Theoretical analysis indicated that, depending on particle diameter, the electrical adhesion force could reach 62.5–1000 pN if the particle carries a charge of 0.5–$2.5 \cdot 10^{-9}$ Cu. In such cases, even 10 μm particles carrying a charge of $2.5 \cdot 10^{-9}$ C may significantly enhance adhesion in a multi-channel cyclone upon entering the first channel under harsh gas flow conditions, since the electrical adhesion force (62.5–250 pN) exceeds the centrifugal adhesion force. However, particles can acquire such high charges only when exposed to a specially created discharge field, e.g., in an electrostatic filter. For comparison, in a discharge field, quartz particles acquire a charge of $0.32 \cdot 10^{-12}$ Cu, while polymer particles can acquire significantly higher charges of up to $3 \cdot 10^{-5}$ Cu. Considering these cases, it can be concluded that electrical adhesion forces acting on fine particles do not significantly increase adhesion within the multi-channel cyclone. the adhesion of agglomerates consisting of small particles is less likely [50].

Experimental Research on Gas Flow Dynamics in Different Design Multi-Channel

Table 4. After conducting experimental studies of the aerodynamic characteristics, the average dynamic pressures in the cyclone channels were determined at the following inlet velocities: cylindrical – 21.9 m/s and spiral – 17.8 m/s. The results are presented in Table 4.

Table 4. Changes in dynamic pressure in the cyclones of cylindrical and spiral shells depending on the positions and geometry of curvilinear semi-rings.

Average dynamic pressures at positions I, II, and III of the semicircular segments, Pa	I channel	II channel	III channel	IV channel	V channel	VI channel	Axial
Cylindrical cyclone with continuous semicircular segments	60.1	71.5	101.9	125.1	157.8	176.8	224.4
	57.7	72.8	100.2	127.5	157.1	179.2	222.6
	55.9	74.5	100.8	128.8	156.8	180.1	220.5
Cylindrical cyclone with semicircular segments containing openings	61.0	72.5	103.5	125.5	158.5	177.0	**225.1**
	58.7	74.0	101.7	128.0	157.7	179.5	223.6
	57.5	75.5	101.5	129.0	157.0	**180.3**	221.8

 doi:10.20944/preprints202604.1464.v1

Spiral cyclone with continuous semicircular segments	57.7	62.2	66.3	78.8	99.8	177.3	187.0
	57.1	60.8	67.5	78.0	101.0	176.5	183.8
	56.1	59.6	68.6	77.2	103.2	175.0	181.3
Spiral cyclone with semicircular segments containing openings	58.4	62.8	67.1	79.2	100.1	**177.5**	**187.5**
	57.6	61.6	68.2	78.5	101.4	176.8	184.5
	56.8	60.3	69.3	77.8	103.5	175.1	182.3

Dynamic pressures were measured at the points indicated in Figure 1, within each channel, in the spaces between the curvilinear elements (at mid-distance). All data were grouped by the corresponding channels, and average values of the dynamic pressures were calculated. It was observed that higher dynamic pressures were recorded in the cylindrical cyclone. Although the volume of the cylindrical cyclone is more than 7.3 times larger than that of the spiral cyclone, the installed fan, operated at maximum power, generates a higher flow. The maximum dynamic pressure was measured at the third semicircular segment position in the sixth channel of the cylindrical cyclone, reaching 180.3 Pa. In contrast, in the spiral cyclone, the maximum value was recorded at the first semicircular segment position in the sixth channel, equal to 177.5 Pa. For other semicircular segment positions, the values measured in the sixth channel were: cylindrical cyclone – 177.0 Pa and 179.5 Pa (first and second positions), and spiral cyclone – 176.8 Pa and 175.1 Pa.

The maximum dynamic pressures inside the cyclone structures were recorded along the device axes in six channels. The highest values were found in the cylindrical cyclone, with a peak of 225.1 Pa, whereas in the spiral cyclone, the corresponding value was only 187.5 Pa. The results indicate that as the gas flow moves from one cyclone channel to another, the average dynamic pressure changes by approximately 1.05–1.45 times, due to the reduction in channel cross-section, which increases both dynamic pressure and velocity.

The motion of the swirling flow is influenced by the variable spin-inducing design of the spiral cyclone. This design feature causes noticeable differences in dynamic pressures when the positions of the curvilinear elements are altered. In the spiral cyclone, the dynamic pressures are highest in the first and even-numbered channels (II, IV, VI) at the first semicircular segment position, while in the odd-numbered channels (III, V) the maximum pressures occur at the third position. Conversely, in the cylindrical cyclone, the highest dynamic pressures in the even-numbered channels are observed at the third position, and in the odd-numbered channels at the first position.

The aerodynamic resistances of the cleaning devices were measured depending on the internal arrangement of semicircular segments with the fans operating at nominal power. Based on the experimental results, it can be concluded that the devices generate low resistance. The maximum pressure for the cylindrical cyclone, at an inlet velocity of 21.9 m/s, reached only 432 Pa, while for the spiral cyclone, at an inlet velocity of 17.8 m/s, it was 382 Pa. Changing the positions of the semicircular segments alters the aerodynamic resistance depending on the flow direction. The highest resistance in the cylindrical cyclone was observed at the first segment position, i.e., when the segments were shifted 10 mm from the second position toward the tangential inlet deflector (Figure 8).

 doi:10.20944/preprints202604.1464.v1

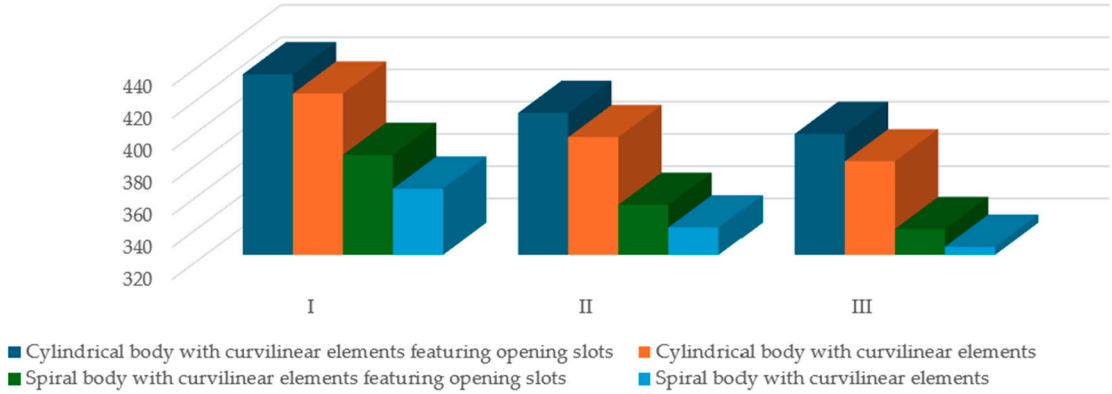

Figure 8. The dependence of aerodynamic resistance of cyclones on the types and positions of curvilinear elements.

As the distance from the inlet deflector wall increases to the right, at the second semicircular segment position, the maximum aerodynamic resistance is generated – 408 Pa, while at the third position the minimum is observed – 395 Pa. A similar trend is observed in the spiral cyclone, where arranging the semicircular segments in the second position produces a maximum resistance of 351 Pa, and in the third position – 336 Pa. The presence of opening slots in the curvilinear elements (semicircular segments) contributes to resistance, increasing it by an average of approximately 4%. However, this geometric modification also enhances filtration efficiency and, consequently, the overall cleaning performance of the device.

Cyclone resistance arises due to flow deceleration, the generation of centrifugal forces, wall friction, and internal fluid flow friction. Among these, the first two losses are most significant, and therefore calculations typically consider only their effects.

The study investigated the cleaning efficiency of six-channel cylindrical and spiral cyclones for gas flow contaminated with the particles. The concentrations of the test glass and clay particles were determined gravimetrically. During the experiments, particle concentrations before cleaning were varied from 500 mg/m³ to 15 g/m³. The objective was to assess the degree of particle separation at different concentrations and to compare the performance of the improved six-channel cyclones.

For determining concentrations and efficiency, the maximum inlet velocity was 21.9 m/s for the cylindrical cyclone and 17.8 m/s for the spiral cyclone. Cleaning efficiency tests were conducted under optimal conditions, with the curvilinear elements set to the second position. The study examined the cleaning efficiency of six-channel cyclones for fine particles (up to 20 μm) and different internal geometries, using both continuous curvilinear elements and curvilinear elements featuring opening slots.

During the tests with curvilinear elements featuring opening slots, the improvement allowed the contaminated gas flow to re-enter the preceding channel, enabling additional particles to settle and enter the collection hopper through the segmented ring gaps (Figure 1).

By measuring the concentrations of glass particles in the ducts before and after cleaning, the maximum cleaning efficiency for the spiral cyclone was 87.3% at a particle concentration of 15 g/m³ using the improved curvilinear elements featuring opening slots. Under the same conditions, the cylindrical cyclone achieved an efficiency of 78.4%. Across different inlet concentrations, the relative performance of the cyclones remained fairly consistent. On average, the spiral cyclone's cleaning efficiency was 11.3% higher than that of the cylindrical cyclone.

The lowest efficiency was recorded at a 500 mg/m³ concentration of glass particles: 48.5% for the cylindrical cyclone and 53.1% for the spiral cyclone. For conventional internal geometry using continuous curvilinear elements, the maximum cleaning efficiency also occurred at the highest inlet concentration (15 g/m³), reaching 81.7% for the spiral cyclone and 74.1% for the cylindrical cyclone.

 doi:10.20944/preprints202604.1464.v1

The minimum efficiency, as noted, was 48.5% (spiral) and 53.1% (cylindrical) at the 500 mg/m³ inlet concentration (Figure 9).

Previous studies by Mothes et al. (1988) demonstrated that cyclone performance improves at higher particle concentrations due to particle agglomeration.

Comparing experimental results for clay particles, the highest cleaning efficiency was also observed at the maximum inlet concentration (15 g/m³) but was lower than that for glass particles. In the cylindrical cyclone, using continuous segments, efficiency reached 64.5%, while with curvilinear elements featuring opening slots it was 69.3%, corresponding to reductions of 1.16 and 1.13 times relative to glass particles. In the spiral cyclone, the efficiency difference between cyclones was 20% with continuous segments (68.1% efficiency) and 18% with curvilinear elements featuring opening slots (74.1% efficiency) (Figure 10).

Analysis of fine particle capture indicates that, in both cyclones, clay particles are collected less efficiently than glass particles. However, the separation efficiency across particle types is more uniform in the cylindrical cyclone than in the spiral cyclone.

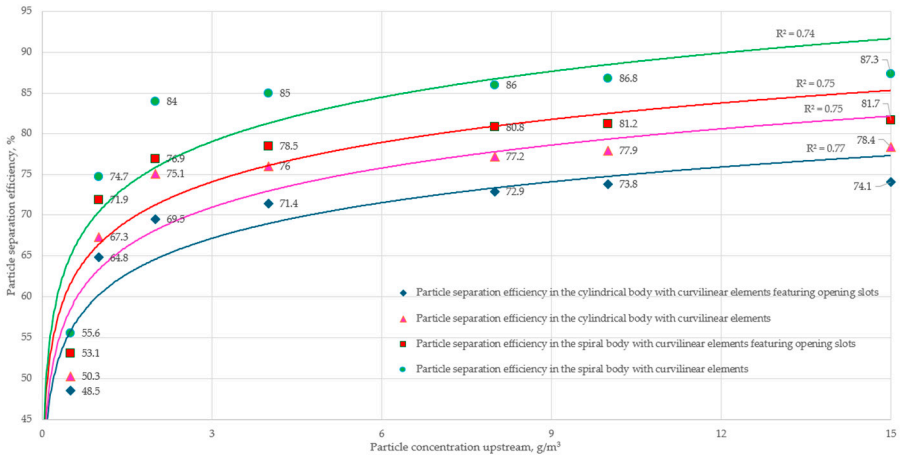

Figure 9. Gas cleaning efficiency of six-channel cyclones of cylindrical and spiral shells depending on the concentration of the glass particles and the internal geometry of the device.

As the uniform in the cylindrical cyclone than in the spiral cyclone.

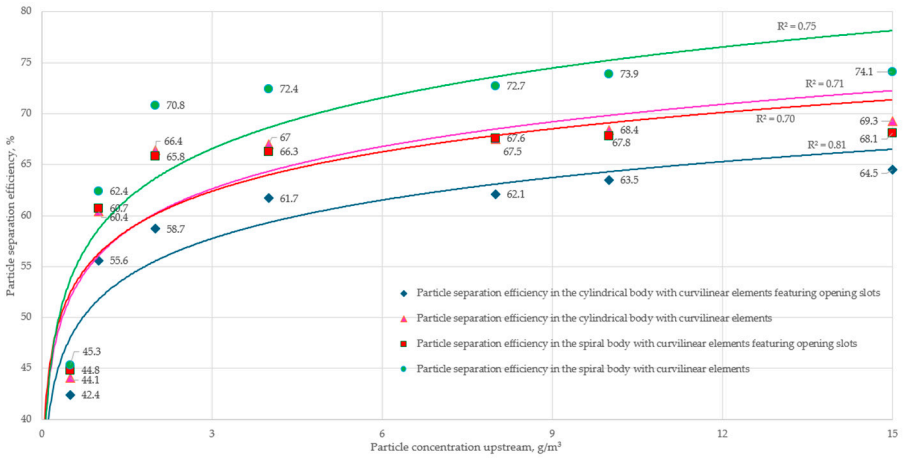

Figure 10. Gas cleaning efficiency of six-channel cyclones of cylindrical and spiral shells depending on the concentration of clay particles and the internal geometry of the device.

When examining cyclones of different housings and internal geometries, the average cleaning efficiency for gas flow containing glass and clay particles differs by a factor of 1.17.

 doi:10.20944/preprints202604.1464.v1

The maximum gas cleaning efficiency for clay particles using continuous semicircular segments in the cylindrical cyclone is 64.5%, which is 9.6% lower than that for glass particles. In the spiral cyclone, the corresponding efficiency values are 68.1% and 13.6%. The trend of efficiency dependence on particle concentration remains consistent: separation efficiency increases with increasing concentration.

Using curvilinear elements featuring opening slots, the cleaning efficiencies for glass and clay particles in both cyclone designs differ by a factor of 1.07. This segment design provided the greatest improvement in cleaning efficiency when applied in the cylindrical cyclone, particularly for the separation of clay particles.

4. Discussion

When cleaning harsh gas flows, high temperature and elevated humidity alter both aerodynamic (e.g., gas velocity) and physical (e.g., viscosity) parameters, thereby affecting cyclone separation efficiency. Under these conditions, the gas flow becomes saturated with moisture, enhancing particle agglomeration, adhesion forces with the internal elements of the multichannel cyclone, and auto-adhesion forces among the fine particles agglomerates themselves. Collectively, these factors create a gas–vapor environment that can clog the segmental ring gaps and openings in the curvilinear elements of the separation chamber, rendering the device inoperable.

In the initial stage of fine particles deposition, monolayers composed of fine particles, which smooth the surfaces where laminar gas flow develops, exhibiting minimal dispersive effects on the deposits. As the deposits accumulate, larger particles may embed within this layer, compacting the formed structures.

Large-scale multichannel cyclones are capable of capturing fine particles due to additional inertial forces acting near the surfaces. These forces arise during turbulent transport of particles when high gradients of pulsating particle velocities are directed toward the surfaces. However, in large cyclones, the adhesion of particle agglomerates composed of fine solids near surfaces is less probable due to reduced centrifugal accelerations (Gong & Wang, 2004).

As contaminated gas enters the multichannel cyclone's separation chamber, fine particles agglomerates adhere to the vertical walls in the cyclone's curved sections. Depending on the mass and spatial distribution of these agglomerates across the cyclone's inlet cross-section, deposition of fine particles is uneven, resulting in surface irregularities.

In order to account for the characteristics of harsh gas flows, simplified theoretical expressions were developed to determine gas density and viscosity. These expressions consider parameters such as partial pressures of dry gas, saturated vapors, and water vapor. Parameter values were selected to represent extreme operating conditions, i.e., maximum possible temperature and humidity of the incoming gas.

In theoretical analyses, the moist gas/vapor mixture is treated as an ideal gas mixture, where the total density equals the sum of the individual component densities. Under this assumption, the density deviation is less than 0.2% over a temperature range of –10 °C to 50 °C. It is also assumed that the relative humidity of the gas flow is inversely proportional to temperature.

Experimental studies have shown that the density of a moist gas flow under harsh conditions is directly proportional to the sum of the partial pressures of dry gas and water vapor and inversely proportional to temperature.

The densities of dry and moist gas flows under harsh gas flow conditions were calculated over a temperature range of 0–200 °C with a step of 25 °C. For moist gas calculations, the maximum relative humidity was assumed to be 95%. For cases where the gas temperature exceeded 100 °C, the relative humidity was computed based on the ratio of atmospheric to saturated water vapor pressure. It was assumed that the pressure inside the multichannel cyclone is constant and equal to atmospheric pressure. Theoretical results are presented in Figure 11.

At lower gas flow temperatures of 25 °C and 50 °C, the density of the dry gas decreases by 9% and 18%, respectively, relative to the density at standard conditions (0 °C), while the density of moist

 doi:10.20944/preprints202604.1464.v1

gas decreases by 7% and 11%, respectively. The partial pressure of saturated vapors increased more than 3.9 times when the temperature changed from 25 °C to 50 °C. At a gas temperature of 100 °C and 95% relative humidity, the density of the moist gas flow is 1.525 kg/m³, while the density of the dry gas flow is 0.945 kg/m³.

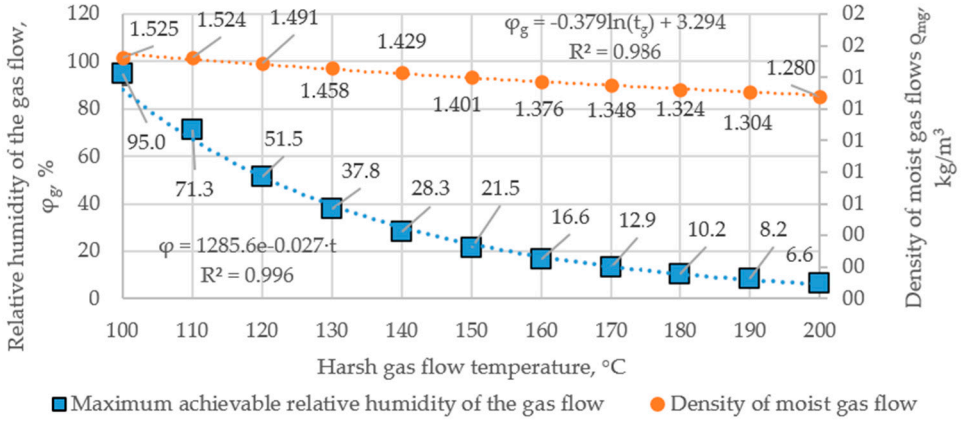

Figure 11. The dependence of the maximum theoretical relative humidity and moist gas flow density (ϱ_{mg}) on gas flow temperature.

As the gas flow temperature rises above 101.7 °C, the maximum achievable relative humidity drops below 95%. The exponentially increasing saturated water vapor pressure contributes to a decrease in both the relative humidity and the density of the moist gas flow. At 120 °C, the relative humidity falls to 51.5%, and at 140 °C and 160 °C, it further decreases to 28.3% and 16.6%, respectively. The saturated water vapor pressure increases 6.1-fold as the temperature rises from 100 °C to 160 °C, reaching 611.7 kPa. The density of dry gas continues to decrease gradually within the 150–200 °C range, reaching 0.745 kg/m³ at 200 °C. For the moist gas, the density within the 160–180 °C range is 1.376–1.324 kg/m³, while the relative humidity at 180 °C is 10.2 % and at 190 °C is 8.2%. At a gas temperature of 200 °C, the relative humidity of the moist gas flow decreases to 6.6%, with a corresponding density of 1.280 kg/m³, while the theoretically determined saturated water vapor pressure increases to 1529.6 kPa. Achieving such a pressure under practical conditions is possible but requires multi-stage heating systems and vessels specifically designed to withstand high pressures. Additionally, a deaerator operating at 1400–1800 kPa must be integrated with the heating system.

When the gas flow temperature exceeds 100 °C, similar trends in density changes for moist and dry gas flows are observed. For every 10 °C increase in temperature, the density of the moist gas decreases by approximately 1%, while the dry gas density decreases by about 2%. The partial pressure of saturated vapor rises sharply with temperature, exhibiting near-exponential growth; for instance, from 100 °C to 200 °C, the pressure increases by a factor of 15.2.

Based on the studies by Lawrence [51] and Wallace and Hobbs [52], it has been established that as the temperature of the gas flow increases, relative humidity decreases exponentially. Theoretical calculations assumed that the critical relative humidity of 95% is maintained at 101.7 °C, corresponding to a saturated water vapor pressure of 106.7 kPa.

Available literature provides data on the variation of relative humidity in gas flows at low temperatures (up to 50 °C) [53]. However, since multichannel cyclones operate at temperatures above 100 °C, these data are insufficient. Therefore, theoretical analyses were conducted, resulting in an approximate mathematical expression (Equation 11) describing the variation of relative humidity in gas flows at temperatures exceeding 100 °C.

$$\varphi_g = 1285.6 \cdot e^{-0.027 \cdot t_g},\ \%, \quad (11)$$

here: φ_g – gas flow relative humidity, %, t_g – gas flow temperature, °C, e = 2.718.

 doi:10.20944/preprints202604.1464.v1

Special conditions influence the density of the gas flow, which is closely related to its viscosity and determines the flow behavior within the cyclone channels. For theoretical calculations, a simplified scenario was selected in which the gas flow consisted of a mixture of gas and water vapor.

Theoretical studies were conducted to derive an expression for the density of the gas flow under harsh microclimatic conditions. Sensitivity analysis indicated that the smallest average deviation occurred between the gas flow density and relative humidity parameters at a temperature of 50 °C, with a value of ±0.24 °C. Based on these results, Equation 12 can be specifically created in a simplified form for calculating the density of gas flows under harsh microclimatic conditions.

$$\rho_g = x_1 \cdot \varphi_g + y_1, \quad (12)$$

if t_g = 20 °C, x_1 = 0.0002, y_1 = 1.2048; if t_g = 50 °C, x_1 = 0.0008, y_1 = 1.093; if t_g = 100 °C, x_1 = 0.0061, y_1 = 0.946; if t_g = 200 °C, x_1 = 0.0809, y_1 = 0.7463;

here: ϱ_g – gas flow density, kg/m³; $\varphi_{d.s.}$ – gas flow relative humidity, %; This expression can be applied when the gas flow temperature is constant, $t_g = const$, °C, x_1 – the first variable of density; y_1 – the second variable of density.

The calculation accuracy was determined by applying different values of the gas flow relative humidity. The deviation for the applied Equation 12 ranged from –0.22% (when φ_g = 95%) to +0.02% (when φ_g = 0%).

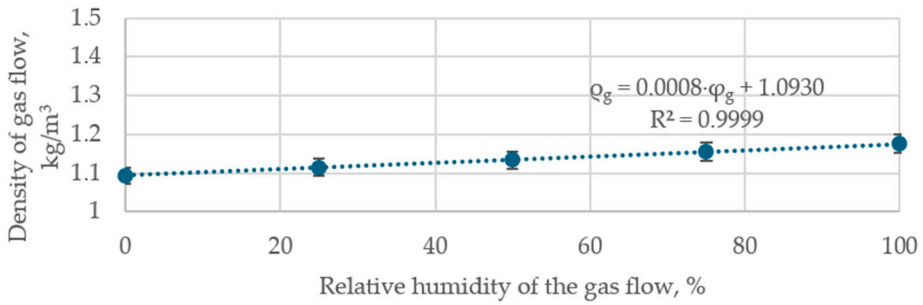

Figure 12. Dependence of gas density on gas flow relative humidity at 50 °C under harsh conditions.

The maximum deviation of the gas flow density values is 0.22%, which indicates that the accuracy of using equation 3.2 for calculating the gas density is sufficient.

Analysis of the particle separation efficiency indicates that gas flow contaminated with clay particles is not as effectively cleaned by the studied device. This is likely due to specific particle properties such as density, shape, degree of agglomeration, and specific surface area. Studies on conventional cyclone designs showed that at high particle concentrations, the effectiveness of centrifugal separation decreases due to the attenuation of the swirling flow and enhanced particle–particle interactions, leading to reduced separation efficiency in cyclones [54–56].

The arrangement of curvilinear elements within the six-channel cyclone affects the system's aerodynamic properties, including dynamic pressure, gas flow velocity, and aerodynamic resistance. Reducing the gaps between the segments and the peripheral walls increases the acting dynamic forces, which in turn modifies other flow parameters. Changes in dynamic pressures influence particle capture efficiency, as particles are transported to the collection hopper through the segmental ring gaps at the bottom by a continuous flow. The measured distribution of dynamic pressures confirms the aerodynamic behavior described in the literature and verified experimentally, allowing for identification of design characteristics, potential defects, and opportunities for further optimization of the device.

Increasing the inlet particle concentration results in higher cleaning efficiency due to the stronger action of centrifugal forces. The six-channel cyclone design is particularly effective because a dynamic gas–dust layer forms in the gaps between the curvilinear elements. As contaminated gas flow passes through this layer, a portion of the particles is retained, thereby enhancing the overall separation efficiency.

 doi:10.20944/preprints202604.1464.v1

5. Conclusions

The present experimental investigation was dedicated to analyzing the aerodynamic characteristics of gas flow in both cylindrical and spiral cyclone shells, which are specifically designed for the separation of fine particles from tangentially introduced gas flows. Special emphasis was placed on examining the distribution of dynamic pressure within the six-channel cyclone configurations. Furthermore, the study assessed the efficiency of particle removal under varying flow phase conditions and when different types of fine particles were introduced, providing comprehensive insight into the performance of these cyclone systems.

1. Harsh environmental factors, such as high temperature in water vapor–saturated flows, have a significant effect on gas properties. Under these conditions, the density and kinematic viscosity of dry gas decrease proportionally, while the density and dynamic viscosity of humid gas increase. At 200 °C and 70% relative humidity, the density of the humid gas flow increases 4.5 times, and its kinematic viscosity rises 3.1 times compared to standard conditions.
2. Analysis of forces acting on particles within the multi-channel cyclone revealed that drag force are among the most significant. At standard conditions, this force is 1.07 mN, whereas at 200 °C and 70% relative humidity, it increases approximately 55%, reaching 2.37 mN. The largest variations were observed at 150 °C and higher temperatures under high humidity conditions (70–80%). Fouling of the multi-channel cyclone system by fine particles is primarily influenced by adhesion forces, while particle deposition is dominated by gravity. For fine particles with diameters below 5 μm, adhesion forces exceed gravitational forces significantly. For 1–2 μm particles, the force ratio is 24–7.5 times, while for 5–10 μm particles, the ratio decreases to 1.8–2.1. The maximum gravitational force, 41.1 pN, acts on 20 μm particles, whereas adhesion accounts for only 11.68% (4.8 pN) of this value.
3. Experimental measurements of dynamic pressures in cyclones indicated a maximum value of 180.3 Pa in the sixth channel of the cylindrical cyclone, compared to 177.5 Pa in the spiral cyclone. The maximum aerodynamic resistance of the spiral cyclone reached 382 Pa, while the cylindrical cyclone exhibited 432 Pa. The arrangement and geometry of curvilinear elements significantly influence aerodynamic resistance, increasing it near the inlet deflector wall under Position I and when curvilinear elements featuring opening slots are employed.
4. Gas purification efficiency experiments were conducted using glass and clay particles up to 20 μm, which conventional cyclone designs typically fail to separate. Using glass particles, the spiral cyclone with curvilinear elements achieved a maximum removal efficiency of 87.3% at an inlet concentration of 15 g/m³. The cylindrical cyclone under the same conditions showed an efficiency 11.3% lower, with a maximum of 78.4%. For clay particles, the highest separation efficiency reached 74.1% in the spiral cyclone using curvilinear elements at 15 g/m³ inlet concentration. In the cylindrical cyclone, the maximum efficiency was 69.3%, approximately 13% lower.
5. Calculations indicated that 10 μm particles in gas flow under harsh microclimatic conditions are predominantly influenced by centrifugal–filtration forces in peripheral flow regions and by adhesion–capillary forces in transitional flow zones. The centrifugal–filtration force reaches up to 600 pN, whereas the adhesion–capillary force is roughly 3.2 times weaker. Compared to standard conditions (0 °C temperature, 50% relative humidity), the density of humid gas decreases from 1.295 kg/m³ to 1.280 kg/m³, the dynamic viscosity increases from 17.17 μPa·s to 24.99 μPa·s, and the kinematic viscosity rises from 13.25 mm²/s to 19.52 mm²/s.

This study is part of the investigation of the fundamental principles and the development of improved cyclone separator designs. The unique geometry and specific operating conditions should be investigated in greater detail in future studies, not only experimentally but also through numerical simulations. It is particularly important to develop models of gas flow dynamics under severe operating conditions. This involves studying the interaction between particle and gas flows, as well as with tertiary phases such as condensate droplets of varying chemical composition and physical

 doi:10.20944/preprints202604.1464.v1

properties in regions where transitional and peripheral flows intersect. The investigation of pressure variations and pressure balance within the device channels, aimed at improving the efficiency of polydisperse particle separation, would enable energy-efficient optimization of the distribution of primary and secondary flows, as well as a reduction in operational losses.

Funding: Not applicable.

Data Availability Statement: The raw data supporting the conclusions of this article will be made available by the authors on request.

Acknowledgments: This project has received funding from the Research Council of Lithuania (LMTLT), agreement No [S-MIP-24-88].

Conflicts of Interest: The author declares no conflicts of interest.

References

1. Aylı, E.; Kocak, E. A Comprehensive Review of Cyclone Separator Technology. *The Canadian Journal of Chemical Engineering* **2024**, *103*, doi:10.1002/cjce.25526.
2. Nakhaei, M.; Lu, B.; Tian, Y.; Wang, W.; Dam-Johansen, K.; Wu, H. CFD Modeling of Gas–Solid Cyclone Separators at Ambient and Elevated Temperatures. *Processes* **2020**, *8*, 228, doi:10.3390/pr8020228.
3. Yang, L.H.; Chen, C.Y.; Hsu, W.Y.; Fukui, K.; Fukasawa, T.; Huang, A.N.; Kuo, H.P. Effect of the Operation Temperature on the Hydrodynamics and Performances of a Cyclone Separator. *Advanced Powder Technology* **2022**, *33*, 103791, doi:10.1016/j.apt.2022.103791.
4. Kang, H.-M.; Yook, S.-J.; Jung, H.-Y. Development and Performance Evaluation of a Rotating Liquid-Cone Cyclone Separator for Enhanced Particle Collection Efficiency. *Separation and Purification Technology* **2026**, *394*, 137615, doi:10.1016/j.seppur.2026.137615.
5. Liang, C.; Ji, Z.; Wu, X. Study on the Influence of Cone Length in Volute-Type Cyclone Separators on Flow Field Characteristics and Energy Consumption. *Separation and Purification Technology* **2026**, *392*, 137032, doi:10.1016/j.seppur.2026.137032.
6. Parker, M.J.; Savory, E.; Straatman, A.G. Development of a Compact Cyclone Particle Separator. *Separation and Purification Technology* **2026**, *393*, 137198, doi:10.1016/j.seppur.2026.137198.
7. Hu, B.; Chen, J.-Y.; Yang, L.-X.; Wu, X.-J.; Wei, Y.-D. Experimental Study on Fine Particle Transport and Deposition Processes in the Swirling Flow of a Cyclone Separator. *Advanced Powder Technology* **2026**, *37*, 105213, doi:10.1016/j.apt.2026.105213.
8. Wang, Z.; Jin, A.; Liu, M. Simulation and Experimental Design of an Axial Flow Cyclone Separator Suitable for High-Wind–Sand Environments. *Sustainability* **2025**, *17*, 3355, doi:10.3390/su17083355.
9. Li, B.; Gao, L.; Li, Y.; Zhu, K.; Fu, Z.; Xu, S.; Li, M. Review on the Optimal Design of Cyclone Separator: Theory, Methodology, and Applications. *Frontiers in Heat and Mass Transfer* **2026**, 1–10, doi:10.32604/fhmt.2026.075814.
10. Wang, M.; Feng, D.; Wang, J.; Hou, L.; Miao, E. CFD Investigation on the Performance of Cyclone Separators with Divergent or Convergent Insertion Pipes. *Processes* **2023**, *11*, 2061, doi:10.3390/pr11072061.
11. Babu, K.S.; Sivapirakasam, S.P.; Venkatesh, S. CFD-Based Evaluation of Performance Enhancement in a Baffle-Integrated Settling Chamber Coupled with a Cyclone Separator. *Powder Technology* **2026**, *469*, 121767, doi:10.1016/j.powtec.2025.121767.
12. Meng, H.; Chen, J.-Y.; Cao, M.-Q.; Hao, Y.-C.; Cui, H.; Yang, L.-X.; Wei, Y.-D. An Experimental Study on the Effect of Interstage Inlet Gas on Separation Performance of Two-Stage Series Cyclone Separators. *Powder Technology* **2024**, *446*, 120147, doi:10.1016/j.powtec.2024.120147.
13. Suppini, C.; Bocelli, M.; Lysova, N.; Volpi, A.; Solari, F.; Montanari, R. A Multi-Stage Classification Approach for Predictive Maintenance of a Cyclonic Bag Filter. *Procedia Computer Science* **2026**, *277*, 3497–3508, doi:10.1016/j.procs.2026.02.385.

 doi:10.20944/preprints202604.1464.v1

14. Yel Mahi, M.; Cremaschi, L. Numerical Analysis of Air Dehumidification through Electrospray-Enhanced Vortical Flow Cyclone Separator. *International Communications in Heat and Mass Transfer* **2025**, *167*, 109253, doi:10.1016/j.icheatmasstransfer.2025.109253.
15. Li, Y.; Qin, G.; Xiong, Z.; Ji, Y.F.; Fan, L. The Effect of Particle Humidity on Separation Efficiency for an Axial Cyclone Separator. *Advanced Powder Technology* **2019**, *30*, 724–731, doi:10.1016/j.apt.2019.01.002.
16. Rosa, E.S.; França, F.A.; Ribeiro, G.S. The Cyclone Gas–Liquid Separator: Operation and Mechanistic Modeling. *Journal of Petroleum Science and Engineering* **2001**, *32*, 87–101, doi:10.1016/S0920-4105(01)00152-8.
17. Muteba, G.K.; Cremaschi, L. Electro-Cyclonic Air Dehumidification Using High-Voltage Electrospray Charging, Dielectrophoresis, and Cyclone Separation. *Journal of Building Engineering* **2026**, *124*, 115884, doi:10.1016/j.jobe.2026.115884.
18. Yuan, S.; Sun, G.; Cao, G.; Wu, Y.; Yue, Y.; Song, Z. Study of the Performance and Flow Field of a New Spiral-Roof Cyclone Separator. *Powder Technology* **2024**, *438*, 119605, doi:10.1016/j.powtec.2024.119605.
19. Koçak, E. System-Level Prediction and Optimization of Cyclone Separator Performance Using a Hybrid CFD–DEM–ANN Approach. *Applied Sciences* **2026**, *16*, 1621, doi:10.3390/app16031621.
20. Barua, S.; Bin Rahim, M.Z.; Liu, Q. Multi-Objective Optimisation of Dual Inlet Cyclone Separator Using Response Surface Methodology. *Particuology* **2026**, *109*, 45–58, doi:10.1016/j.partic.2025.12.004.
21. Dehdarinejad, E.; Moradi, A.; Jahangiri, M.; Dehdarinejad, M. Analysis and Multi-Objective Optimization Impact of the Helical Guide Baffle and Wall Roughness on the Cyclone Performance Using SVR and MOABC Algorithms. *Chemical Engineering Science* **2026**, *325*, 123394, doi:10.1016/j.ces.2026.123394.
22. Edoardo, B.; Piero, D.; Massimo, M.; Li, Z. Generalization of a Semi-Empirical Model to Predict the Efficiency Curve of Laboratory- and Industrial-Scale Cyclone Separators. *Separation and Purification Technology* **2026**, *388*, 136385, doi:10.1016/j.seppur.2025.136385.
23. Li, K.; Zhang, D.; Xie, L.; Zhu, G. Multi-Objective Optimization of Swirler in Gas-Liquid Cyclone Separator for Aircraft Environment Control System. *Applied Thermal Engineering* **2026**, *294*, 130563, doi:10.1016/j.applthermaleng.2026.130563.
24. Zhang, X.; Ma, S.; Wang, X.; He, Z.; Chang, Y.; Jiang, X. Energy-Efficient Design of Cyclone Separators: Machine Learning Prediction of Particle Self-Rotation Velocities. *Energy* **2025**, *316*, 134452, doi:10.1016/j.energy.2025.134452.
25. Elshorbagy, K.A.; Mohammed, E.A.; AbdElKader, M.G. Particle Sphericity Effects on Tangential Velocity and Pressure Drop in Particulate Matter Cyclone Separators: A CFD–Machine Learning Integrated Study. *Powder Technology* **2026**, *476*, 122407, doi:10.1016/j.powtec.2026.122407.
26. Yao, Y.; Shang, M.; Ke, X.; Zhang, J.; Huang, Z.; Zhou, T.; Lyu, J. Design of Multi-Stage Contracted Inlet Duct for Cyclone Separators. *Separation and Purification Technology* **2024**, *332*, 125753, doi:10.1016/j.seppur.2023.125753.
27. Wang, C.M.; Wang, T.F.; Fukui, K.; Fukasawa, T.; Hsu, W.Y.; Huang, A.N.; Kuo, H.P. Novel Entrance and Exit Designs towards Fully Developed Dual Vortexes in Cyclone Separators. *Advanced Powder Technology* **2025**, *36*, 104937, doi:10.1016/j.apt.2025.104937.
28. Pukkella, A.K.; Cilliers, J.; Hadler, K. Design of Parabolic Conic Gas Cyclones for Coarse Particle Classification: A CFD Study with Response Surface Methodology. *Powder Technology* **2024**, *433*, 119217, doi:10.1016/j.powtec.2023.119217.
29. Duan, J.; Gao, S.; Hou, C.; Wang, W.; Zhang, P.; Li, C. Effect of Cylinder Vortex Stabilizer on Separator Performance of the Stairmand Cyclone. *Powder Technology* **2020**, *372*, 305–316, doi:10.1016/j.powtec.2020.06.031.
30. Sun, Z.; Yang, H.; Zhang, K.; Wang, Z.; Hong, Z.; Yang, G. Self-Cleaning Effect and Secondary Swirling Clean Gas for Suppressing Particle Deposition on Vortex Finder of Gas Cyclones. *Particuology* **2024**, *90*, 72–87, doi:10.1016/j.partic.2023.11.021.
31. Zhang, Y.-H.; Liu, A.-L.; Ma, L.; Wang, Y.-M. Acid Mist Cyclone Separation Experiment on the Hydrochloric Acid Regeneration System of a Cold Rolling Steel Plant. *Aerosol and Air Quality Research* **2016**, *16*, 2287–2293, doi:10.4209/aaqr.2016.03.0126.

 doi:10.20944/preprints202604.1464.v1

32. Pacheco, P.; Alves, M.A.; Campos, J.B.L.M.; Paiva, J. Erosion in Stairmand Cyclone by Heavy Spherical Particles: Numerical Modelling with Experimental Validation. *Powder Technology* **2025**, *453*, 120565, doi:10.1016/j.powtec.2024.120565.
33. Salakhova, E.I.; Zinurov, V.E.; Dmitriev, A.V.; Salakhov, I.I. Modeling of Erosion in a Cyclone and a Novel Separator with Arc-Shaped Elements. *Processes* **2023**, *11*, 156, doi:10.3390/pr11010156.
34. Yang, M.; Song, P.; Kong, D.; Huang, T.; Jin, Q. Wear and Corrosion Properties of HVOF Sprayed WC-Cr3C2 Composite Coating for Application in Polysilicon Cyclone Separator. *Journal of Materials Research and Technology* **2024**, *29*, 78–89, doi:10.1016/j.jmrt.2024.01.114.
35. Wang, L.; Chen, E.; Ma, L.; Yang, Z.; Li, Z.; Yang, W.; Wang, H.; Chang, Y. Numerical Simulation and Experimental Study of Gas Cyclone–Liquid Jet Separator for Fine Particle Separation. *Chinese Journal of Chemical Engineering* **2022**, *51*, 43–52, doi:10.1016/j.cjche.2021.12.015.
36. Li, Y.; Jiang, Q.; Yi, T.; Lou, J. Numerical Simulation Method for Steam Water Separator Used in PWR Steam Generator. *Nuclear Engineering and Technology* **2026**, *58*, 104187, doi:10.1016/j.net.2026.104187.
37. Wang, F.; Bi, L.; Yang, X.; Wang, J.; Zhang, Y. Efficient Removal of Particulate Matter through Heterogeneous Condensation, Collision Convergence, and Cyclone Separation: Characteristic and Mechanism. *Separation and Purification Technology* **2025**, *361*, 131374, doi:10.1016/j.seppur.2024.131374.
38. Dimitrijević, D.; Schmid, M.; Harasek, M.; Bösenhofer, M. Comparison of Experimental, Empirical, and CFD Pressure Losses of Lab-Scale Sampling Cyclones. *Separation and Purification Technology* **2025**, *354*, 128992, doi:10.1016/j.seppur.2024.128992.
39. Dehdarinejad, E.; Bayareh, M. Performance Analysis of a Novel Cyclone Separator Using RBFNN and MOPSO Algorithms. *Powder Technology* **2023**, *426*, 118663, doi:10.1016/j.powtec.2023.118663.
40. Beloconi, A.; Vounatsou, P. Revised EU and WHO Air Quality Thresholds: Where Does Europe Stand? *Atmospheric Environment* **2023**, *314*, 120110, doi:10.1016/j.atmosenv.2023.120110.
41. Vázquez Calvo, V.L.; Korzeb, Z.; Alonso-Fariñas, B.; Morillo Aguado, J. Circular Economy Transition under the Revised Industrial Emissions Directive: A Review of Challenges and Enablers. *Journal of Cleaner Production* **2025**, *533*, 146779, doi:10.1016/j.jclepro.2025.146779.
42. Kasman, A.; Kasman, S.; Yildirim, B. Convergence of Air Pollution-Related Death Rates across EU Countries. *Atmospheric Pollution Research* **2024**, *15*, 102196, doi:10.1016/j.apr.2024.102196.
43. Zinurov, V.E.; Dmitrieva, O.S.; Popkova, O.S. Collecting Finely-Dispersed Particles from the Gas Flow in a Centrifugal Separator with Coaxially Arranged Pipes. *MATEC Web Conf.* **2020**, *315*, 03003, doi:10.1051/matecconf/202031503003.
44. Jasevičius, R.; Kruggel-Emden, H.; Baltrėnas, P. Numerical Simulation of the Sticking Process of Glass-Microparticles to a Flat Wall to Represent Pollutant-Particles Treatment in a Multi-Channel Cyclone. *Particuology* **2017**, *32*, 112–131, doi:10.1016/j.partic.2016.09.009.
45. Baltrėnas, P.; Leonavičienė, T. Modelling Trajectories of Solid Particle Motion in the Cyclone. *EC* **2017**, *34*, 1829–1848, doi:10.1108/EC-12-2015-0393.
46. Jasevičius, R.; Kruggel-Emden, H.; Baltrėnas, P. Numerical Simulation of the Sticking Process of Glass-Microparticles to a Flat Wall to Represent Pollutant-Particles Treatment in a Multi-Channel Cyclone. *Particuology* **2017**, *32*, 112–131, doi:10.1016/j.partic.2016.09.009.
47. Jasevičius, R.; Baltrenas, P.; Kačianauskas, R.; Grubliauskas, R. DEM Simulation of the Impact of Ultrafine Glass Particles on the Partition Wall of the Multichannel Cyclone. *Particulate Science and Technology* **2014**, *32*, doi:10.1080/02726351.2014.933145.
48. Cao, G.; Sun, J.; Sun, G.; Zhou, F.; Fu, S. Influence of a Spiral Guide Vane on the Flow Field and Particle Deposition Outside the Vortex Finder of FCC Disengager Cyclone Separators. *Energy* **2025**, *337*, 138593, doi:10.1016/j.energy.2025.138593.
49. Zhou, F.; Xing, Y.; Guo, Y.; Wang, X.; Xu, J.; Wang, D. Fine Particle Deposition on the Outer Wall of the Vortex Finder in Cyclone Separator: Modeling with Particle Rotational Effects. *Separation and Purification Technology* **2026**, *380*, 135461, doi:10.1016/j.seppur.2025.135461.
50. Gong, A.; Wang, L.-Z. Numerical Study of Gas Phase Flow in Cyclones with the Repds. *Aerosol Science and Technology* **2010**, *May 2004*, 506–512, doi:10.1080/02786820490449548.

 doi:10.20944/preprints202604.1464.v1

51. Lawrence, M. The Relationship between Relative Humidity and the Dewpoint Temperature in Moist Air: A Simple Conversion and Applications. *Bulletin of the American Meteorological Society* **2005**, *86*, 225–234, doi:10.1175/BAMS-86-2-225.
52. Wallace, J.M.; Hobbs, P.V. Atmospheric Science: An Introductory Survey: Second Edition; 2006; p. 488;.
53. Moisture Handbook. Machine Applications Corporation.
54. Kumar, V.; Jha, K. Effects of Mass-Loading on Performance of the Cyclone Separators. In *Applications of Computational Fluid Dynamics Simulation and Modeling*; IntechOpen, 2022 ISBN 978-1-83968-248-3.
55. Zhang, Y.; Yang, M.; Jiang, L.; Wang, H.; Xu, J.; Yang, J. High Concentration Fine Particle Separation Performance in Hydrocyclones. *Minerals* **2021**, *11*, doi:10.3390/min11030307.
56. Misiulia, D.; Antonyuk, S.; Andersson, A.G.; Lundström, T.S. High-Efficiency Industrial Cyclone Separator: A CFD Study. *Powder Technology* **2020**, *364*, 943–953, doi:10.1016/j.powtec.2019.10.064.